HHS Public Access

Author manuscript

NMR Biomed. Author manuscript; available in PMC 2024 February 01.

Published in final edited form as:

NMR Biomed. 2023 February ; 36(2): e4844. doi:10.1002/nbm.4844.

4D Golden-Angle Radial MRI at Subsecond Temporal Resolution

Li Feng

Biomedical Engineering and Imaging Institute and Department of Radiology, Icahn School of Medicine at Mount Sinai, New York, NY, United States

Abstract

Intra-frame motion blurring, as a major challenge in free-breathing dynamic MRI, can be reduced if high temporal resolution can be achieved. To address this challenge, this work proposes a highly-accelerated 4D (3D+time) dynamic MRI framework with sub-second temporal resolution that does not require explicit motion compensation. The method combines standard stack-of-stars golden-angle radial sampling and tailored GRASP-Pro (Golden-angle RAdial Sparse Parallel) reconstruction. Specifically, 4D dynamic MRI acquisition is performed continuously without motion gating or sorting. The k-space centers in stack-of-stars radial data are organized to guide estimation of a temporal basis, with which GRASP-Pro reconstruction is employed to enforce joint low-rank subspace and sparsity constraints. This new basis estimation strategy is the new feature proposed for subspace-based reconstruction in this work to achieve high temporal resolution (e.g., sub-second/3D volume). It does not require sequence modification to acquire additional navigation data; it is compatible with commercially available stack-of-stars sequences, and it does not need an intermediate reconstruction step. The proposed 4D dynamic MRI approach was tested in abdominal motion phantom, free-breathing abdominal MRI, and dynamic contrast-enhanced MRI (DCE-MRI). Our results have shown that GRASP-Pro reconstruction with the new basis estimation strategy enabled highly-accelerated 4D dynamic imaging at sub-second temporal resolution (with 5 spokes or less for each dynamic frame per image slice) for both free-breathing non-DCE-MRI and DCE-MRI. In the abdominal phantom, better image quality with lower RMSE and higher SSIM was achieved using GRASP-Pro compared to standard GRASP reconstruction. With the ability to acquire each 3D image in less than one second, intra-frame respiratory blurring can be intrinsically reduced for body applications with our approach, which also eliminates the need for motion detection and motion compensation.

Graphical Abstract

This work proposes a highly-accelerated 4D (3D+time) dynamic MRI framework with sub-second temporal resolution combining standard stack-of-stars golden-angle radial sampling and tailored GRASP-Pro (Golden-angle RAdial Sparse Parallel) reconstruction. Image reconstruction is performed using a combination of low-rank subspace and sparsity constraints, where a temporal basis is estimated from the stack-of-stars k-space centers to guide image reconstruction.

Address correspondence to: Li Feng, PhD, Biomedical Engineering and Imaging Institute, Department of Radiology, Icahn School of Medicine at Mount Sinai, 1470 Madison Ave, New York, NY, USA 10029, lifeng.mri@gmail.com.

Disclosure

Li Feng is a co-inventor of a patent on the GRASP MRI technique.

Keywords

GRASP; GRASP-Pro; Dynamic MRI; Radial Sampling; Stack-of-Stars; Subspace; DCE-MRI; Motion Correction

Introduction

High-performance volumetric MRI (3D MRI) in presence of respiratory motion has been a challenging task. Due to the slow acquisition speed in MRI, state-of-the-art free-breathing volumetric imaging methods typically rely on triggering, gating, registration-based motion correction, motion-weighted reconstruction, or motion-resolved reconstruction to reduce respiration-induced motion blurring or artifacts within an image[1–5] (referred to as intra-frame blurring in dynamic imaging). To date, these approaches still suffer from different challenges and limitations at varying degrees, such as reduced imaging efficiency, compromised image quality under irregular breathing, and sensitivity to motion drifts. In the meantime, these approaches also require accurate information about the underlying respiratory motion pattern (typically obtained through a motion detection process) for motion compensation. Inaccurate motion detection can lead to poor motion compensation, yielding residual motion artifacts. Currently, motion detection is commonly performed with external motion sensors (e.g., a respiratory bellow or pilot tone[6,7]) or with self-navigation[8–12]. For dynamic contrast-enhanced MRI (DCE-MRI), respiratory motion detection can be much more challenging due to the change of image contrast along time; and therefore, the detected motion signal can be contaminated by contrast variation[4,13]. This potentially reduces the accuracy and robustness of motion detection in free-breathing DCE-MRI, which constitutes a major restriction for its wide clinical translation.

Stack-of-stars golden-angle radial sampling has emerged as a promising hybrid acquisition trajectory (in-plane radial sampling + through-plane Cartesian sampling) for free-breathing MRI and DCE-MRI[14,15]. In radial imaging, motion artifacts typically spread through the entire field of view (FOV) as blurring, and adequate image quality has been demonstrated even with mild motion blurring[16–18]. Besides, radial sampling provides good incoherence that can be exploited with sparse reconstruction techniques for fast data acceleration[19,20], and the golden-angle rotation scheme enables continuous data acquisition with flexibility to reconstruct dynamic images with arbitrary temporal resolution[14,21,22]. Combining stack-of-stars golden-angle radial sampling with multicoil compressed sensing reconstruction, a method called GRASP (Golden-angle RAdial Sparse Parallel imaging) has been developed for rapid free-breathing dynamic MRI[22], and it has been applied to a number of clinical applications[18,23–27]. While GRASP ensures good image quality in some body applications such as prostate and breast imaging, it still results in compromised image quality with residual motion blurring for applications with large motion displacement, such as liver and lung imaging[13,28]. To address this challenge, GRASP has been extended to XD-GRASP (eXtral-Dimensional GRASP), which performs data sorting based on underlying motion information and then sparse reconstruction to generate motion-resolved dynamic images[4]. XD-GRASP has been applied to both non-DCE-MRI[29–31] and DCE-MRI applications[32], and it has also shown great potential for use in image-guided treatment planning[33]. However,

like other motion compensation techniques, a major challenge in XD-GRASP is the requirement for reliable motion detection, which could be challenging in some applications such as DCE-MRI. Meanwhile, the need to reconstruct a new respiratory dimension also limits the achievable temporal resolution in DCE-MRI with XD-GRASP.

If temporal resolution is high enough to resolve respiratory motion, standard 4D dynamic MRI (3D+time) acquired in real time is sufficient to address these challenges without the need for explicit motion compensation. Here, the term “real-time acquisition” refers to data acquisition at specific time points during underlying physical dynamics (e.g., motion) without sorting and/or gating, and it should not be confused with real-time reconstruction or real-time imaging with low latency[34]. For example, given that a standard respiratory cycle typically spans for 4–6 seconds, it is fair enough to assume minimum respiratory motion blurring within each image if one can acquire a 3D image in an order of millisecond. In the same way, 4D dynamic MRI with sub-second temporal resolution can capture respiration-induced signal variation and ensure minimal intra-frame blurring. Unfortunately, standard MRI, even with the state-of-the-art accelerated imaging techniques available in the clinic, is still not fast enough to achieve this goal. Currently, most dynamic MRI applications with real-time acquisition are performed based on 2D imaging[35–40], and compromised spatiotemporal resolution is often needed for 3D/4D imaging[41–44]. The achievable temporal resolution in 4D dynamic MRI with real-time acquisition using standard acceleration techniques (e.g., GRASP) is typically in an order of seconds[23], which is sensitive to intra-frame motion for moving organs such as the liver.

More recently, an improved version of GRASP reconstruction, called GRASP-Pro[45], has been proposed to improve image quality and temporal resolution over GRASP. GRASP-Pro extends GRASP with joint low-rank subspace and sparsity constraints, where the temporal basis used for subspace construction is estimated from an intermediate GRASP reconstruction using low-resolution k-space data. However, with its original implementation, GRASP-Pro still requires sufficient data (radial spokes in each dynamic frame) to ensure good reconstruction performance for the intermediate step, which inherently limits the achievable temporal resolution to fully resolve intra-frame blurring. In this work, we sought to further tailor GRASP-Pro reconstruction for 4D stack-of-stars MRI towards high temporal resolution below one second. Compared to the original GRASP-Pro implementation and other subspace-based reconstruction methods, the main innovation in our optimization is to estimate the temporal basis from the centers of stack-of-stars k-space. With this simple but effective extension, GRASP-Pro breaks the restrictions associated with the intermediate reconstruction step required in its original implementation; and it is compatible with standard stack-of-stars acquisition. This ultimately leads to a new dynamic MRI framework that enables 4D MRI at sub-second temporal resolution, which intrinsically reduces intra-frame respiratory motion blurring for body applications and eliminates the need for motion detection and motion compensation.

Methods

GRASP-Pro Reconstruction with K-Space Center-Guided Basis Estimation

With stack-of-stars golden-angle radial sampling, GRASP MRI reconstruction can be implemented in a slice-by-slice matter (either sequential or parallelized), where 2D dynamic image reconstruction is performed for each slice. The use of golden-angle rotation enables flexible data sorting and grouping to reconstruct dynamic images with arbitrary temporal resolution. Standard GRASP implements multicoil compressed sensing reconstruction to solve the following optimization problem:

$$\widetilde{\mathbf{m}} = \arg\min_{\widetilde{\mathbf{m}}} \frac{1}{2}\left\|\mathbf{Em} - \sqrt{\mathbf{W}}\mathbf{y}\right\|_2^2 + \lambda_t\|\mathbf{S_t m}\|_1 + \lambda_s\|\mathbf{S_s m}\|_1 \quad [1]$$

Here, $\mathbf{m} \in \mathbf{C}^{T \times N^{\wedge}2}$ is the dynamic image series to be reconstructed with an in-plane matrix size of $N \times N$ for each dynamic frame and a number of T dynamic frames. $\mathbf{y}$ is corresponding multicoil dynamic k-space. $\mathbf{S_t}$ is a temporal sparsifying transform (e.g., temporal finite differences) applied along the dynamic dimension and $\mathbf{S_s}$ is a spatial sparsifying transform (e.g., spatial finite differences) applied to each dynamic frame separately. λ_t and λ_s are two parameters for the two regularization terms, respectively. In the latest implementation of GRASP reconstruction, self-calibrating GeneRalized Autocalibrating Partial Parallel Acquisition (GRAPPA) Operator Gridding, known as GROG[46], is applied to speed up image reconstruction, where $\mathbf{W}$ is a GROG weighting matrix as described by Benkert T et al[47]. $\mathbf{E} = \sqrt{\mathbf{W}}\mathbf{FC}$ represents the encoding operator for multicoil reconstruction combining coil sensitivities ($\mathbf{C}$), fast Fourier transform (FFT: $\mathbf{F}$) and $\mathbf{W}$.

The use of generic sparisfying transforms to minimize L_1 norm in standard GRASP reconstruction limits its achievable acceleration rates, which poses a trade-off between temporal resolution and image quality. To improve reconstruction quality while having high temporal resolution, GRASP has been extended to GRASP-Pro to enforce joint low-rank subspace and sparsity constraints[45]. Specifically, GRASP-Pro aims to solve the following optimization problem:

$$\widetilde{\mathbf{V}}_{\mathbf{K}} = \arg\min_{\widetilde{\mathbf{V}}_{\mathbf{K}}} \frac{1}{2}\left\|\mathbf{E}(\mathbf{U_K V_K}) - \sqrt{\mathbf{W}}\mathbf{y}\right\|_2^2 + \lambda_1\|\mathbf{S_t}(\mathbf{U_K V_K})\|_1 + \lambda_2\|\mathbf{S_s V_K}\|_1 \quad [2]$$

Here, $\mathbf{U_K} \in \mathbf{C}^{T \times K}$ refers to the K ($K << T$) dominant basis components taken form the full basis $\mathbf{U} \in \mathbf{C}^{T \times T}$. $\mathbf{V_K} \in \mathbf{C}^{K \times N^{\wedge}2}$ refers to the spatial basis, or spatial characteristics corresponding to $\mathbf{U_K}$ for representing the dynamic image series to be reconstructed. Optimization of Equation 2 aims to reconstruct $\mathbf{V_K}$, and the dynamic images to be reconstructed ($\mathbf{m}$) are then given as $\mathbf{U_K V_K} \in \mathbf{C}^{T \times N^2}$. The improved reconstruction performance using GRASP-Pro, compared to standard GRASP, is mainly attributed to the reduced degrees of freedom from the construction of a subspace in iterative reconstruction[48], as one only needs to reconstruct K images ($\mathbf{V_K}$) instead of the original T images ($\mathbf{m}$). An

important step to perform subspace-constrained reconstruction is to pre-estimate **U** before iterative reconstruction. Although some studies have also proposed to solve both $\mathbf{U_K}$ and $\mathbf{V_K}$ jointly in iterative reconstruction[49,50], this will likely make the optimization problem non-convex and increase the reconstruction complexity substantially.

In the original implementation of GRASP-Pro, **U** is pre-estimated in an intermediate reconstruction step using standard GRASP performed on the low-resolution k-space data[45]. However, the need for this intermediate reconstruction step inherently limits achievable acceleration rates and thus achievable temporal resolution, since sufficient k-space data (radial spokes included in each dynamic frame) are still needed for the low-resolution GRASP reconstruction to minimize error in basis estimation. Meanwhile, this extra reconstruction step also requires an additional reconstruction step that prolongs total computation time.

Instead of estimating the temporal basis from an intermediate reconstruction step as described above, we propose to estimate the basis from the k-space centers in stack-of-stars k-space data, which is then used for GRASP-Pro reconstruction. As shown in Figure 1a, stack-of-stars sampling offers a unique feature, with which a number of k-space centers (purple circles) are acquired in a radial stack. Here, a radial stack is formed by all the spokes from all slices at a given acquisition angle. While the acquisition angle keeps rotating from one stack to the next, the centers of k-space are repeatedly sampled at the same locations. These k-space centers can be transformed to a series of projections with 1D FFT along the slice dimension to obtain underlying information, such as respiratory motion and/or contrast enhancement, as shown in Figure 1b. These projections can be re-organized to match the target temporal resolution by grouping and averaging consecutive projections together. For example, when every 5 consecutive spokes are combined for image reconstruction, every 5 consecutive projections are also averaged for basis estimation. The temporal basis can then be estimated using principal component analysis (PCA):

$$\mathbf{Proj} = \mathbf{U}\mathbf{V}_{\mathbf{proj}} \quad [3]$$

Here, $\mathbf{Proj} \in \mathbf{C}^{T\times ZC}$ represents concatenated multicoil projections generated from k-space centers of all coil elements, where Z indicates the number of partitions/slices in stack-of-stars k-space data and $\mathbf{V_{proj}} \in \mathbf{C}^{K\times ZC}$ refers to as the coefficients corresponding to the estimated basis. Given the estimated **U**, the K dominant basis components can be extracted to generate $\mathbf{U_K} \in \mathbf{C}^{T\times K}$ for GRASP-Pro reconstruction as outlined in Equation 2. With this approach, one temporal basis is estimated from the projections for the whole image-set, which can be applied to reconstruct all image slices together or separately. For simplicity, when GRASP-Pro reconstruction is mentioned hereafter, it is referred to as the optimized reconstruction method with the new basis estimation scheme.

The temporal basis estimated from k-space central projections is used to represent the dynamic image series to be reconstructed. This is valid because: (1) temporal basis contains only temporal information; (2) although the k-space central projections contains limited spatial information, it properly reflects underlying temporal information that is needed for estimating the temporal basis, and (3) the subspace spanned by the temporal basis is not

limited to represent the data used for estimating the basis (k-space center projections); instead, the basis can be used to represent much more signal patterns as long as they are correlated with the training signals[51]. Figure 1b shows two representative examples of projections, which provide good information reflecting underlying dynamic changes. It should be noted that the feasibility of estimating temporal basis from 1D projections for subspace-constrained reconstruction has been demonstrated in prior studies[51,52]. However, these studies intended to acquire additional 1D navigation data periodically for this purpose, which prolongs overall scan time and needs specific sequence modification. In contrast, the unique sampling feature in the stack-of-stars trajectory enables self-calibration for temporal basis estimation directly from the acquired k-space centers.

Imaging Experiments

Multiple experiments were designed to test the proposed 4D dynamic MRI framework, including numerical motion phantom, free-breathing non-DCE-MRI and DCE-MRI studies in a total of 8 subjects. Lastly, a T1 mapping phantom study was conducted to quantitatively verify the accuracy of basis estimation in GRASP-Pro. Human imaging was HIPAA-compliant and was approved by the local Institutional Review Board (IRB). Written informed consent was obtained from all the subjects prior to their MR scans. MR imaging was performed on 3T clinical MRI scanners (Siemens Magnetom Skyra or Prisma, Erlangen, Germany) using a prototype stack-of-stars imaging sequence (known as StarVIBE or RadialVIBE).

Abdominal Motion Phantom Study—A realistic 4D abdominal motion phantom was simulated to test highly-accelerated 4D MRI using stack-of-stars golden-angle radial sampling and k-space center-guided GRASP-Pro reconstruction. 4D abdominal phantom images were simulated using source code provided by Lo W et al[53]. Imaging parameters for the phantom included: FOV = 380×380mm^2, matrix size = 256×256, number of slices = 40, and slice thickness = 5mm. A total of 196 dynamic frames were simulated to cover 7 full respiratory cycles. Assuming a respiratory cycle of ~6 seconds, this led to a temporal resolution of ~210ms/3D volume. To mimic normal breathing in human, the duration of the expiratory phase is longer than the inspiration phase in each respiratory cycle. Ground truth images were first generated after adding zero-mean Gaussian noise with a signal-to-noise ratio (SNR) of 46dB to the simulated images. Golden-angle stack-of-stars k-space data were then synthesized for each image slice, where each dynamic frame contains 5 consecutive spokes. The rotation angle was set the same for each radial stack to simulate standard stack-of-stars sampling. For each slice, dynamic images were reconstructed using non-uniform FFT (NUFFT), standard GRASP, and GRASP-Pro. For additional comparison, GRASP-Pro reconstruction was also performed using a temporal basis estimated from an intermediate GRASP reconstruction (the original implementation, denoted as GRASP-Pro-orig) and from the ground truth images (denoted as GRASP-Pro-ref), respectively. It should be noted that GRASP-Pro-ref is only available in simulated dataset, since fully sampled references are not available in practice. Root mean square error (RMSE) and structural similarity index (SSIM) were calculated for each dynamic frame with respect to the ground truth.

Non-DCE-MRI Study—4D dynamic MRI was tested in 5 stack-of-stars golden-angle radial abdominal MRI datasets (referred to as non-DCE dataset 1–5) acquired in 4 subjects without contrast injection. All imaging parameters are listed in Table 1.

Non-DCE dataset 1 was acquired in subject 1 (male, age=28) in the axial orientation. For the first comparison, both GRASP reconstruction and GRASP-Pro reconstruction were performed on the dataset to generate 4D dynamic images with 5 consecutive spokes grouped in each dynamic frame for each slice. This resulted in a temporal resolution of 0.78 seconds/3D volume. For the second comparison, XD-GRASP was performed on the dataset to reconstruct 4 respiratory motion-resolved images spanning from end-expiration to end-inspiration, as described previously[4]. The number of spokes for each respiratory phase in the XD-GRASP reconstruction was 162.

Non-DCE dataset 2 was acquired in subject 2 (female, age=32) in the axial orientation, and non-DCE dataset 3 was acquired in subject 3 (male, age=24) in the coronal orientation. GRASP-Pro reconstruction was performed on these two datasets to generate 4D dynamic images with 5 consecutive spokes grouped in each dynamic frame for each slice. This resulted in a temporal resolution of 0.63 seconds/3D volume for dataset 2 and 0.68 seconds/3D volume for dataset 3.

Non-DCE dataset 4 and 5 were both acquired in subject 4 (male, age=27), one in the axial orientation (dataset 4) and the other one in the coronal orientation (dataset 5). For acquisition of both datasets, the volunteer was asked to perform consistent deep breathing as much as possible. GRASP-Pro reconstruction was performed on these two datasets to generate 4D dynamic images with 5 consecutive spokes grouped in each dynamic frame for each slice. This resulted in a temporal resolution of 0.44 seconds/3D volume (70/800*5) and 0.61 seconds/3D volume (159/1304*5). For additional comparison, XD-GRASP was performed on dataset 4 to reconstruct 6 respiratory phases spanning from expiration to inspiration.

DCE-MRI Study—4D dynamic MRI was also tested in 4 stack-of-stars golden-angle radial MRI datasets acquired in 4 subjects following the injection of a Gadolinium-based contrast agent (referred to as DCE dataset 1–4). All imaging parameters are listed in Table 1.

DCE dataset 1 was acquired in the liver of subject 1 (female, age=28) in the axial orientation. For the first comparison, GRASP and motion-weighted GRASP reconstruction[13] was first performed with 96 consecutive spokes grouped in each dynamic frame for each slice with a temporal resolution = 15 seconds/3D volume. GRASP-Pro reconstruction was then performed with 5 consecutive spokes grouped for each dynamic frame for each slice with a temporal resolution of 0.78 seconds/3D volume. For the second comparison, the temporal resolution was further pushed to 0.47 seconds/3D volume with only 3 consecutive spokes grouped in each dynamic frame for each slice. The low-rank plus sparsity (L+S) reconstruction[54] was additional performed for comparison using MATLAB code provided by the authors.

DCE dataset 2 was acquired in the lung of subject 2 (female, age=34) in the axial orientation. DCE dataset 3 was acquired in the prostate of subject 3 (male, age=61) in the axial orientation. For these two datasets, GRASP-Pro reconstruction was performed to generate 4D dynamic images with 5 consecutive spokes grouped in each dynamic frame for each slice with a temporal resolution 0.76 seconds/3D volume (lung) and 0.63 seconds/3D volume (prostate).

DCE dataset 4 was performed in the liver of subject 4 (female, age=57) in the axial orientation. The subject had irregular breathing pattern during the MR imaging. GRASP-Pro reconstruction was performed on the dataset to generate 4D dynamic images with 5 consecutive spokes combined in each dynamic frame for each slice with a temporal resolution of 0.78 seconds/3D volume. For additional comparison, GRASP reconstruction and motion-weighted GRASP reconstruction[13] were also performed in this dataset both with a temporal resolution of 15 seconds/3D volume (96 consecutive spokes in each dynamic frame for each slice).

To assess the temporal fidelity of compressed sensing reconstruction in DCE-MRI, we previously proposed to use NUFFT as an indirect reference[22]. This is based on the observation that without any temporal regularization, NUFFT images can still preserve the true temporal fidelity despite the presence of streaking artifacts, especially with region-of-interest (ROI)-based analysis. In this study, NUFFT images were also used as a reference to assess the temporal fidelity of GRASP-Pro reconstruction. However, given that NUFFT reconstruction with high acceleration rates has substantial streaking artifacts, it was performed with a lower temporal resolution compared to GRASP-Pro to reduce the influence of streaking artifacts.

T1 Mapping Phantom Study—To quantitatively verify the accuracy of GRASP-Pro reconstruction using k-space center-guided temporal basis estimation, a T1 mapping phantom dataset with an in-plane matrix size of 256×256 was acquired using inversion-recovery (IR) prepared stack-of-stars sampling with 17 IR repetitions as described in[55]. The acquisition for the T1 mapping phantom was not in real time, but it was mainly used to assess the accuracy of k-space center-guided basis estimation. The dataset was reconstructed using GRASP-Pro reconstruction with temporal basis estimated from the Bloch simulation (served as reference) and k-space centers, respectively.

Implementation of Image Reconstruction—All image reconstruction tasks were performed in MATLAB (MathWorks, MA) with GPU implementation by using the “gpuArray” function. Radial k-space data were prepared using the unstreaking technique in a pre-processing step to improve image quality[13,56]. Self-calibrating GROG was implemented to replace NUFFT for iterative reconstruction to improve reconstruction speed[46,47].

Results

Abdominal Motion Phantom Study

Results comparing NUFFT, GRASP, GRASP-Pro reconstruction with different basis estimation schemes and the ground truth for one slice of the abdominal motion phantom, along with corresponding x-t temporal profiles, are presented in Figure 2. With only 5 spokes per dynamic frame, NUFFT reconstruction yielded substantial streaking artifacts and GRASP failed to remove those artifacts. GRASP-Pro reconstruction, in comparison, was able to generate substantially improved image quality and there is no visual difference between GRASP-Pro and GRASP-Pro-ref. While GRASP-Pro-orig can still achieve much improved image quality compared to GRASP, the result suffers from residual streaking artifacts. This may be because the basis for subspace construction in GRASP-Pro-orig was estimated from an intermediate reconstruction step on low-resolution k-space using GRASP, and the performance of GRASP can be limited at this accelerated rate. Thus, errors generated in basis estimation are likely propagated to the final reconstructed images. The RMSE and SSIM results indicate that the expiratory motion phases can reconstructed better than the inspiratory phases. This is likely due to reduced temporal correlations in inspiratory phase compared to expiratory phase as simulated in the phantom dataset. Cine movies corresponding to Figure 2 are shown in the Supporting Documents (Video 1).

Non-DCE-MRI Study

Results comparing NUFFT, GRASP and GRASP-Pro reconstruction for 4D dynamic MRI with a temporal resolution of 0.78 seconds/3D volume are shown for non-DCE dataset 1 in Figure 3. NUFFT reconstruction produced strong streaking artifacts at this accelerate rate. Although GRASP could remove many of those artifacts, the reconstruction quality remains low. In comparison, GRASP-Pro was able to generate clean and sharp images with good delineation of image structures in different dynamic frames. Cine movies corresponding to Figure 3 are shown in the Supporting Documents (Video 2).

For the same dataset, Figure 4 compares motion-averaged images reconstructed using NUFFT (all 650 spokes), GRASP-Pro with 5 spokes grouped in each dynamic frame (a total of 130 dynamic frames) and XD-GRASP with 4 respiratory-resolved phases (162 spokes in each phase). Compared to the motion-averaged NUFFT reconstruction, both GRASP-Pro and XD-GRASP reconstruction yielded improved image sharpness as indicated by the better delineation of vessel-tissue boundaries. However, the inspiratory images reconstructed with XD-GRASP is slightly better than corresponding images reconstructed with GRASP-Pro, while the expiratory images are more comparable. This is consistent with that observed in the motion phantom study (see Figure 2) considering the fact that the expiratory duration is normally longer in human breathing pattern.

Figure 5 shows 4D dynamic MR images reconstructed using GRASP-Pro in non-DCE dataset 2 (axial imaging) and dataset 3 (coronal imaging). Images are displayed for an expiratory phase and an inspiratory phase from 2 slices. With the sub-second temporal resolution (0.63 seconds/3D volume and 0.68 seconds/3D volume), intra-frame blurring is reduced without the need of explicit motion compensation, while good image quality can be

preserved. Cine movies corresponding to Figure 5b are shown in the Supporting Documents (Video 3).

Figure 6 shows 4D dynamic MR images reconstructed using GRASP-Pro in non-DCE dataset 4 and dataset 5 with consistent deep breathing. Images are displayed for an expiratory phase and an inspiratory phase. With a temporal resolution of 0.44 seconds/3D volume and 0.61 seconds/3D volume, strong motion blurring is presented in the motion-averaged images, which can be largely reduced with GRASP-Pro reconstruction. However, it was noted that the overall image quality of these two datasets is degraded compared to normal breathing. Figure 7 compares XD-GRASP with GRASP-Pro in non-DCE dataset 4. Due to deep breathing, XD-GRASP with the typical 6 motion-phase reconstruction is insufficient to fully resolve respiratory motion, while GRASP-Pro with a sub-second temporal resolution was able to recover more details in the liver.

DCE-MRI Study

Figure 8 compares standard GRASP reconstruction and motion-weighted GRASP reconstruction with a temporal resolution of 15 seconds/3D volume with GRASP-Pro reconstruction with sub-second temporal resolution (0.78 seconds/3D volume) in DCE dataset 1. GRASP-Pro reconstruction did not implement any motion compensation algorithm and the expiratory phases in different contrast enhanced phases are displayed. Despite much more aggressive acceleration, GRASP-Pro reconstruction yielded good reconstruction quality that is comparable to motion-weighted GRASP reconstruction. Standard GRASP reconstruction suffers from residual motion blurring as indicated by the blurred hepatic vessels (yellow arrows). Cine movies corresponding to Figure 8 are shown in the Supporting Documents (Video 4). More contrast phases from different slices reconstructed with GRASP-Pro in this dataset are also shown in Figure 9.

Figure 10 compares NUFFT, GRASP, L+S and GRASP-Pro reconstruction for 4D dynamic MRI with a temporal resolution of 0.47 seconds/3D volume in DCE dataset 1. Images are displayed for a pre-contrast phase, an arterial phase, a venous phase and a delayed phase. Compared to different reference methods, GRASP-Pro was able to reconstruct clean and sharp images with good delineation of image structures in different contrast-enhanced phases despite vast acceleration. Cine movies corresponding to Figure 10 are shown in the Supporting Documents (Video 5).

Figure 11 shows GRASP-Pro reconstruction in DCE dataset 2 (upper panel, lung imaging) and DCE dataset 3 (lower panel, prostate imaging). The results clearly demonstrate the recovery of image quality from NUFFT reconstruction with 5 spokes per temporal frame in each slice. Cine movies corresponding to Figure 11 are shown in the Supporting Documents (Video 6). Figure 12 compares the contrast enhancement curves in different ROIs between NUFFT and GRASP-Pro reconstruction in DCE dataset 1–3 (a-c). As described in the method section, the temporal resolution of the NUFFT reconstruction was set much lower than GRASP-Pro to have sufficient image quality as a reference for assessing temporal fidelity. That is why the NUFFT curves show larger step size and some temporal blurring.

Figure 13 shows images reconstructed with GRASP-Pro in DCE dataset 4. While the subject had irregular breathing during data acquisition (as shown by the projections in Figure 13a), GRASP-Pro was able to reconstructed good images in different contrast phases with a temporal resolution of 0.78 seconds/3D volume in each slice, which clearly differentiate different motion phases in a respiratory cycle (Figure 13b). Comparison of GRASP and motion-weighted GRASP reconstruction with a temporal resolution of 15 seconds/3D volume with GRASP-Pro reconstruction with sub-second temporal resolution (0.78 seconds/3D volume) in a venous phase from this dataset is shown in Figure 13c. The GRASP image shows residual blurring. While motion-weighted reconstruction improved the overall image quality, the delineation of small vessels is still slightly compromised compared to GRASP-Pro, as indicated by the yellow arrows, which is likely due to residual intra-frame motion blurring and low temporal resolution.

T1 Mapping Phantom Study

Finally, Figure 14 compares T1 maps generated from images reconstructed with GRASP-Pro using a temporal basis estimated from a dictionary generated using the Bloch equations and a temporal basis estimated from the centers of k-space. There is no visual difference in the T1 maps, which is confirmed by the quantitative analysis of mean T1 values in different phantom vials. The linear correlation analysis yielded an R^2 of 0.999, and the Lin's Concordance Correlation Coefficient (CCC) was excellent (0.9994). These results have quantitatively shown that k-space center-guided basis estimation can be accurate for subspace reconstruction.

Discussion

In this study, an MRI framework is proposed to enable 4D dynamic MRI with sub-second temporal resolution. This is achieved with a combination of stack-of-stars golden-angle radial sampling and GRASP-Pro reconstruction that is tailored for temporal basis estimation. With GPU implementation, the time needed to reconstruct each image slice was about ~2–3 minutes. The performance of our imaging technique has been demonstrated in experiments in numerical motion phantom and multiple in-vivo datasets, and it has been compared against state-of-the-art motion-compensation methods based on motion-resolved reconstruction and motion-weighted reconstruction. The significance of performing 4D dynamic MRI at sub-second temporal resolution goes beyond pushing imaging speed. Importantly, it provides a simple and effective way to perform fast free-breathing dynamic imaging that does not require specific sequence modification, does not require motion detection, and can intrinsically address intra-frame respiratory blurring.

Sparse image reconstruction with subspace constrains can be performed in different ways. The temporal basis that is needed for subspace construction can either be pre-estimated before iterative reconstruction or jointly reconstructed together with the to-be-reconstructed image series. Pre-estimation of the basis has some advantages, as it can simplify and accelerate the reconstruction process compared to joint basis-image reconstruction, which tends to be non-convex, complex, and slow. The pre-estimation of the basis has been proposed based on (a) fully-sampled low-resolution k-space region[48], (b) additionally

acquired navigation data[51], or (c) an intermediate reconstruction step on undersampled low-resolution k-space region[45]. The estimation scheme (a) has several major limitations, including the need for specific sequence modification and prolonged scan time to acquire k-space center, which limits achievable acceleration rate and temporal resolution. Meanwhile, it is mainly implemented for Cartesian sampling and can become problematic in others such as radial sampling. The main limitation of the estimation scheme (b) is the need of additional time to acquire navigation data for basis estimation, and this also requires specific modification to the imaging sequence. The estimation scheme (c) was proposed in the original implementation of GRASP-Pro reconstruction. It is simple and does not need sequence adaption. However, the main restriction of this scheme is the need to have sufficient data for the intermediate reconstruction. Any reconstruction errors, such as temporal blurring or residual undersampling artifacts, can be propagated to the final reconstructed images. As a result, this requirement limits achievable temporal resolution as shown in our experiments (Figure 2). To overcome these limitations, the main contribution of this study is to show that one can estimate a temporal basis from the centers of k-space in stack-of-stars imaging. This simple extension nicely breaks the restrictions in estimation scheme (c) and enables highly-accelerated data acquisition and thus exquisite temporal resolution to address intra-frame motion blurring.

Stack-of-stars sampling is ideal to perform the proposed 4D dynamic imaging, as the k-space centers are repeatedly sampling to form z-directional projections for basis estimation. Therefore, it provides a nature way for subspace-constrained reconstruction without the need for sequence modification, which facilitates easy clinical translation and dissemination. The use of k-space centers to guide image reconstruction in stack-of-stars imaging has been demonstrated in many prior studies, but the main use has been limited to motion detection, self-gating or motion sorting[4,10]. However, any gradient error (e.g., gradient delay) can prevent accurate acquisition of k-space center. To improve this situation, 3 or 5 k-space centers from spokes oriented from different angles are averaged to minimize potential error. Meanwhile, a high bandwidth (~1000 Hz/pixel) was also used to reduce the readout duration to minimize gradient errors. Another possible solution to address this limitation is to use stack-of-spirals sampling, which has previously been implemented for 4D dynamic MRI using nonlinear inversion[57] and through-time GRAPPA[58]. since the k-space center is sampled as the first point in spiral acquisition, this can ensure more accurate acquisition of the k-space center.

Our study shares some similarities with two recent works on highly-accelerated DCE-MRI. The first one is called extreme MRI[50], which enables 4D dynamic MRI at sub-second temporal resolution using 3D radial sampling and a multiscale low-rank subspace constraint. However, this approach aims to reconstruct basis and images jointly and requires a specific reconstruction algorithm to solve a non-convex optimization problem for 4D MRI reconstruction, which is slow (e.g., 6–42 hours) for clinical translation. Meanwhile, 3D radial trajectories usually require data acquisition with isotropic resolution. Although this is desired in whole-heart imaging, it may not be necessary in many other applications and the computational burden is high[14]. The second one is based on the MR multitasking technique for fast DCE-MRI[52]. This study implemented a 3D variable density undersampled Cartesian trajectory. Additional navigation k-space data were periodically acquired to enable

basis estimation for subspace construction. Meanwhile, this study aimed to reconstruct a six-dimensional image-set including a respiratory motion dimension, which could slow down the overall image reconstruction time. In comparison, our current study implements stack-of-stars sampling and aims to estimate a temporal basis from the centers of k-space without the need for sequence modification. Meanwhile, with stack-of-stars sampling, one can break down the reconstruction task for each slice separately, which can reduce the overall reconstruction burden and speed up the reconstruction process with parallel computing.

The performance of reconstructing an image series from only a few spokes per frame primarily relies on available temporal correlations. As such, our proposed method requires a sufficient number of dynamic frames. Figure 4 has shown that the expiratory image from GRASP-Pro reconstruction (with 5 spokes per dynamic frame) is comparable with XD-GRASP reconstruction (with 162 spokes per motion phase), while the inspiratory image from XD-GRASP reconstruction looks better than GRASP-Pro. This is mainly because the inspiratory duration in a normal breathing cycle is shorter than the expiratory duration. Additional results to show the influence of scan time on GRASP-Pro reconstruction can be seen in the Supporting Document (Supporting Experiment A). In addition, the construction of subspace also plays a key role in reconstructing highly-accelerated dynamic images. As previously demonstrated by Zhao et al[48], subspace-based reconstruction substantially reduces the degrees of freedoms compared to other low-rank reconstruction methods without generating a subspace (e.g., L+S), which explains why GRASP-Pro is superior to L+S as shown in Figure 10. Instead of generating temporal basis using standard PCA, more advanced calibration based on Block-Hankel structure, as demonstrated by Rosenzweig, might provide better performance for subspace-based image reconstruction[59].

Subspace-based image reconstruction needs to determine the size of subspace (the value of K in Equation 2). This parameter, like other subspace reconstruction methods, was empirically selected in this work. This was performed by comparing image reconstruction using different values of K. Specifically, a large K gives better confidence to preserve temporal fidelity, but it will be insufficient to enforce the low-rank condition and thus the reconstruction quality/image quality will be reduced. On the other side, a small K can ensure clean images, but it could also generate temporal blurring by excessively removing high-frequency coefficients. As a result, the value of K has to be carefully selected to achieve a good balance between temporal fidelity and image quality. In this work, K=10 was used for DCE-MRI reconstruction and K= 8 was used for non-DCE-MRI reconstruction. Comparison of images reconstructed with different values of K is shown in the Supporting Document (Supporting Experiment B).

There are several advantages to apply the proposed 4D dynamic MRI method to DCE-MRI, especially in the liver. First, DCE-MRI has to be performed with real-time data acquisition since contrast enhancement is not periodic. Second, DCE-MRI acquisition typically lasts for several minutes, which provides sufficient data to exploit temporal correlations. Third, our method provides a more robust way to address intra-frame respiratory blurring without the need for motion detection. Fourth, as shown in Figure 8, a large number of contrast phases can be reconstructed in DCE-MRI with our method, which offers additional flexibility

(compared to standard GRASP with moderate temporal resolution) to retrospectively choose desired contrast phases. Fifth, it has been reported that the arterial phases in DCE-MRI of the liver are often degraded by respiratory motion due to the quick passage of a contrast agent[60]. By addressing intra-frame respiratory blurring, our method could provide an easy way to address this challenge.

Our proposed 4D dynamic MRI method aims to address intra-frame motion. However, with this target temporal resolution, inter-frame motion (displacement from one dynamic frame to the others caused by respiration) and selection of desired contrast phases from a large number of reconstructed phases for clinical evaluation can become new challenges. It has been previously shown the deep learning could help identify appropriate contrast phases that are needed by radiologists, and it could also help choose respiratory phases from all the phases. This additional extension for automated contrast phase selection will be explored in future works.

The proposed 4D dynamic MRI method can have more applications beyond those demonstrated in this work. It could be applied for imaging moving joints (e.g., wrist or knee) or for imaging speech with volumetric information. Image-guided treatment planning or adaptive radiotherapy is another nice application to use this imaging approach. Without the need of self-gating or motion sorting, additional robustness can be obtained to address potential motion drift in Image-guided treatment. One limitation of the method, however, is that the achieved temporal resolution can only address respiratory motion but not cardiac motion. This is because cardiac motion occurs at a much higher frequency than respiratory motion, which may need a temporal resolution of less than 100ms. As a result, the target application of this imaging method is limited to the body or chest but not the cardiovascular system.

Conclusion

This study proposed a highly-accelerated 4D dynamic MRI framework that combine 3D golden-angle radial stack-of-stars sampling and tailored GRASP-Pro reconstruction to enable sub-second temporal resolution. The ability to acquire a 3D image within one second intrinsically provides a simple but effective method to reduce intra-frame respiratory motion blurring for body applications and eliminates the need for motion detection and motion compensation. The method could potentially be useful for different applications that benefit from real-time data acquisition during free breathing, such as DCE-MRI and image-guided treatment planning.

Supplementary Material

Refer to Web version on PubMed Central for supplementary material.

Acknowledgement

This work was supported in part by the NIH (R01EB030549, R01EB031083, R21EB032917). Early support of this work was derived from NIH P41 EB017183. The author thanks Dr. Tobias Block for sharing the RAVE sequence for T1 mapping and Ding Xia for helping with the phantom experiment.

Grant Support:

NIH R01EB030549, R01EB031083, R21EB032917

List of Abbreviations

MRI	Magnetic Resonance Imaging
DCE-MRI	Dynamic Contrast-Enhanced MRI
FOV	Field of View
GRASP MRI	Golden-angle RAdial Sparse Parallel MRI
XD-GRASP	eXtral-Dimensional GRASP
GRASP-Pro	GRASP with imProved performance
GRAPPA	GeneRalized Autocalibrating Partial Parallel Acquisition
GROG	GRAPPA Operator Gridding
FFT	Fast Fourier Transform
SNR	Signal to Noise Ratio
PCA	Principal Component Analysis
NUFFT	Non-Uniform FFT
RMSE	Root Mean Square Error
SSIM	Structural SIMilarity index
FA	Flip Angle
TE	Echo Time
TR	Repetition Time
SNR	Signal to Noise Ratio
PF	Partial Fourier
L+S	Low-rank plus Sparsity
ROI	Region of Interest
CCC	Concordance Correlation Coefficient

References

1. Zaitsev M, Maclaren J, Herbst M. Motion Artefacts in MRI: a Complex Problem with Many Partial Solutions. J. Magn. Reson. Imaging 2015;42(4):887. Available at: /pmc/articles/PMC4517972/. Accessed February 22, 2022. [PubMed: 25630632]

2. Scott AD, Keegan J, Firmin DN. Motion in Cardiovascular MR Imaging1 10.1148/radiol.2502071998. 2009;250(2):331–351. Available at: https://pubs.rsna.org/doi/10.1148/radiol.2502071998. Accessed June 20, 2022.

3. Cheng JY, Zhang T, Ruangwattanapaisarn N, et al. Free-breathing pediatric MRI with nonrigid motion correction and acceleration. J. Magn. Reson. Imaging 2015;42(2):407–420. Available at: https://onlinelibrary.wiley.com/doi/full/10.1002/jmri.24785. Accessed February 22, 2022. [PubMed: 25329325]

4. Feng L, Axel L, Chandarana H, et al. XD-GRASP: Golden-angle radial MRI with reconstruction of extra motion-state dimensions using compressed sensing. Magn. Reson. Med 2016;75(2):775–788. [PubMed: 25809847]

5. van Heeswijk RB, Bonanno G, Coppo S, et al. Motion Compensation Strategies in Magnetic Resonance Imaging. Crit. Rev. Biomed. Eng 2012;40(2):99–119. Available at: https://www.dl.begellhouse.com/journals/4b27cbfc562e21b8,6e675cde67fa0c72,5f77ce066d9e70a0.html. Accessed June 20, 2022. [PubMed: 22668237]

6. Vahle T, Bacher M, Rigie D, et al. Respiratory Motion Detection and Correction for MR Using the Pilot Tone Applications for MR and Simultaneous PET/MR Examinations 2019. Available at: https://journals.lww.com/investigativeradiology. Accessed February 22, 2022.

7. Falcão MBL, Di Sopra L, Ma L, et al. Pilot tone navigation for respiratory and cardiac motion-resolved free-running 5D flow MRI. Magn. Reson. Med 2022;87(2):718–732. Available at: https://onlinelibrary.wiley.com/doi/full/10.1002/mrm.29023. Accessed March 22, 2022. [PubMed: 34611923]

8. Stehning C, Börnert P, Nehrke K, et al. Free-breathing whole-heart coronary MRA with 3D radial SSFP and self-navigated image reconstruction. Magn. Reson. Med 2005;54(2):476–480. [PubMed: 16032682]

9. Piccini D, Littmann A, Nielles-Vallespin S, et al. Respiratory self-navigation for whole-heart bright-blood coronary MRI: Methods for robust isolation and automatic segmentation of the blood pool. Magn. Reson. Med 2012;68(2):571–579. Available at: https://onlinelibrary.wiley.com/doi/full/10.1002/mrm.23247. Accessed February 22, 2022. [PubMed: 22213169]

10. Liu J, Spincemaille P, Codella NCF, et al. Respiratory and cardiac self-gated free-breathing cardiac CINE imaging with multiecho 3D hybrid radial SSFP acquisition. Magn. Reson. Med 2010;63(5):1230–1237. Available at: https://onlinelibrary.wiley.com/doi/full/10.1002/mrm.22306. Accessed February 22, 2022. [PubMed: 20432294]

11. Pang J, Sharif B, Fan Z, et al. ECG and navigator-free four-dimensional whole-heart coronary MRA for simultaneous visualization of cardiac anatomy and function. Magn. Reson. Med 2014;72(5):1208–1217. [PubMed: 25216287]

12. Larson AC, White RD, Laub G, et al. Self-gated cardiac cine MRI. Magn. Reson. Med 2004;51(1):93–102. Available at: https://pubmed.ncbi.nlm.nih.gov/14705049/. Accessed February 22, 2022. [PubMed: 14705049]

13. Feng L, Huang C, Shanbhogue K, et al. RACER-GRASP: Respiratory-weighted, aortic contrast enhancement-guided and coil-unstreaking golden-angle radial sparse MRI. Magn. Reson. Med 2018;80(1):77–89. [PubMed: 29193260]

14. Feng L Golden-Angle Radial MRI: Basics, Advances, and Applications. J. Magn. Reson. Imaging 2022. Available at: https://onlinelibrary.wiley.com/doi/full/10.1002/jmri.28187. Accessed May 31, 2022.

15. Block KT, Chandarana H, Milla S, et al. Towards Routine Clinical Use of Radial Stack-of-Stars 3D Gradient-Echo Sequences for Reducing Motion Sensitivity. J. Korean Soc. Magn. Reson. Med 2014;18(2):87.

16. Chandarana H, Block KT, Winfeld MJ, et al. Free-breathing contrast-enhanced T1-weighted gradient-echo imaging with radial k-space sampling for paediatric abdominopelvic MRI. Eur. Radiol 2013 242. 2013;24(2):320–326. Available at: https://link.springer.com/article/10.1007/s00330-013-3026-4. Accessed August 16, 2021. [PubMed: 24220754]

17. Chandarana H, Block TK, Rosenkrantz AB, et al. Free-breathing radial 3D fat-suppressed T1-weighted gradient echo sequence: A viable alternative for contrast-enhanced liver imaging in patients unable to suspend respiration. Invest. Radiol 2011;46(10):648–653. Available at: https://journals.lww.com/investigativeradiology/Fulltext/

2011/10000/Free_Breathing_Radial_3D_Fat_Suppressed.7.aspx. Accessed August 16, 2021. [PubMed: 21577119]

18. Chandarana H, Feng L, Block TK, et al. Free-breathing contrast-enhanced multiphase MRI of the liver using a combination of compressed sensing, parallel imaging, and golden-angle radial sampling. Invest. Radiol 2013;48(1):10–16. [PubMed: 23192165]
19. Block KT, Uecker M, Frahm J. Undersampled radial MRI with multiple coils. Iterative image reconstruction using a total variation constraint. Magn. Reson. Med 2007.
20. Adluru G, McGann C, Speier P, et al. Acquisition and reconstruction of undersampled radial data for myocardial perfusion magnetic resonance imaging. J. Magn. Reson. Imaging 2009;29(2):466–473. Available at: https://onlinelibrary.wiley.com/doi/full/10.1002/jmri.21585. Accessed February 22, 2022. [PubMed: 19161204]
21. Winkelmann S, Schaeffter T, Koehler T, et al. An optimal radial profile order based on the golden ratio for time-resolved MRI. IEEE Trans. Med. Imaging 2007;26(1):68–76. [PubMed: 17243585]
22. Feng L, Grimm R, Block KT obia., et al. Golden-angle radial sparse parallel MRI: combination of compressed sensing, parallel imaging, and golden-angle radial sampling for fast and flexible dynamic volumetric MRI. Magn. Reson. Med 2014;72(3):707–717. [PubMed: 24142845]
23. Feng L, Benkert T, Block KT, et al. Compressed sensing for body MRI. J. Magn. Reson. Imaging 2017;45(4):966–987. [PubMed: 27981664]
24. Rosenkrantz AB, Geppert C, Grimm R, et al. Dynamic contrast-enhanced MRI of the prostate with high spatiotemporal resolution using compressed sensing, parallel imaging, and continuous golden-angle radial sampling: Preliminary experience. J. Magn. Reson. Imaging 2015;41(5):1365–1373. Available at: https://onlinelibrary.wiley.com/doi/full/10.1002/jmri.24661. Accessed August 16, 2021. [PubMed: 24833417]
25. Zhang J, Feng L, Otazo R, et al. Rapid dynamic contrast-enhanced MRI for small animals at 7T using 3D ultra-short echo time and golden-angle radial sparse parallel MRI. Magn. Reson. Med 2019;81(1):140–152. [PubMed: 30058079]
26. Kim SG, Feng L, Grimm R, et al. Influence of temporal regularization and radial undersampling factor on compressed sensing reconstruction in dynamic contrast enhanced MRI of the breast. J. Magn. Reson. Imaging 2016;43(1):261–269. Available at: https://onlinelibrary.wiley.com/doi/full/10.1002/jmri.24961. Accessed August 16, 2021. [PubMed: 26032976]
27. Chen L, Liu D, Zhang J, et al. Free-breathing dynamic contrast-enhanced MRI for assessment of pulmonary lesions using golden-angle radial sparse parallel imaging. J. Magn. Reson. Imaging 2018;48(2):459–468. [PubMed: 29437281]
28. Chen L, Zeng X, Ji B, et al. Improving dynamic contrast-enhanced MRI of the lung using motion-weighted sparse reconstruction: Initial experiences in patients. Magn. Reson. Imaging 2020;68:36–44. Available at: https://pubmed.ncbi.nlm.nih.gov/32001328/. Accessed June 20, 2022. [PubMed: 32001328]
29. Piccini D, Feng L, Bonanno G, et al. Four-dimensional respiratory motion-resolved whole heart coronary MR angiography. Magn. Reson. Med 2017;77(4):1473–1484. [PubMed: 27052418]
30. Feng L, Coppo S, Piccini D, et al. 5D whole-heart sparse MRI. Magn. Reson. Med 2018;79(2):826–838. [PubMed: 28497486]
31. Feng L, Delacoste J, Smith D, et al. Simultaneous Evaluation of Lung Anatomy and Ventilation Using 4D Respiratory-Motion-Resolved Ultrashort Echo Time Sparse MRI. J. Magn. Reson. Imaging 2019;49(2):411–422. Available at: https://pubmed.ncbi.nlm.nih.gov/30252989/. Accessed June 30, 2021. [PubMed: 30252989]
32. Chandarana H, Feng L, Ream J, et al. Respiratory motion-resolved compressed sensing reconstruction of free-breathing radial acquisition for dynamic liver magnetic resonance imaging. Invest. Radiol 2015;50(11):749–756. [PubMed: 26146869]
33. Feng L, Tyagi N, Otazo R. MRSIGMA: Magnetic Resonance SIGnature MAtching for real-time volumetric imaging. Magn. Reson. Med 2020;84(3):1280–1292. Available at: https://onlinelibrary.wiley.com/doi/full/10.1002/mrm.28200. Accessed June 20, 2022. [PubMed: 32086858]

34. Dietz B, Fallone BG, Wachowicz K. Nomenclature for real-time magnetic resonance imaging. Magn. Reson. Med 2019;81(3):1483–1484. Available at: https://pubmed.ncbi.nlm.nih.gov/30183101/. Accessed September 29, 2022. [PubMed: 30183101]
35. Holsinger AE, Wright RC, Riederer SJ, et al. Real-time interactive magnetic resonance imaging. Magn. Reson. Med 1990;14(3):547–553. Available at: https://onlinelibrary.wiley.com/doi/full/10.1002/mrm.1910140312. Accessed June 20, 2022. [PubMed: 2355836]
36. Kerr AB, Pauly JM, Hu BS, et al. Real-time interactive MRI on a conventional scanner. Magn. Reson. Med 1997;38(3):355–367. Available at: https://onlinelibrary.wiley.com/doi/full/10.1002/mrm.1910380303. Accessed June 20, 2022. [PubMed: 9339436]
37. Frahm J, Voit D, Uecker M. Real-Time Magnetic Resonance Imaging: Radial Gradient-Echo Sequences With Nonlinear Inverse Reconstruction. Invest. Radiol 2019;54(12):757–766. Available at: https://journals.lww.com/investigativeradiology/Fulltext/2019/12000/Real_Time_Magnetic_Resonance_Imaging__Radial.4.aspx. Accessed June 20, 2022. [PubMed: 31261294]
38. Uecker M, Zhang S, Voit D, et al. Real-time MRI at a resolution of 20 ms. NMR Biomed 2010;23(8):986–994. Available at: https://pubmed.ncbi.nlm.nih.gov/20799371/. Accessed June 20, 2022. [PubMed: 20799371]
39. Seiberlich N, Ehses P, Duerk J, et al. Improved Radial GRAPPA Calibration for Real-Time Free-Breathing Cardiac Imaging. Magn. Reson. Med 2011;65(2):492. Available at: /pmc/articles/PMC3012142/. Accessed June 20, 2022. [PubMed: 20872865]
40. Feng L, Srichai MB, Lim RP, et al. Highly accelerated real-time cardiac cine MRI using k-t SPARSE-SENSE. Magn. Reson. Med 2013;70(1):64–74. [PubMed: 22887290]
41. Burdumy M, Traser L, Burk F, et al. One-second MRI of a three-dimensional vocal tract to measure dynamic articulator modifications. J. Magn. Reson. Imaging 2017;46(1):94–101. Available at: https://onlinelibrary.wiley.com/doi/full/10.1002/jmri.25561. Accessed June 20, 2022. [PubMed: 27943448]
42. Zhao Z, Lim Y, Byrd D, et al. Improved 3D real-time MRI of speech production. Magn. Reson. Med 2021;85(6):3182–3195. Available at: https://onlinelibrary.wiley.com/doi/full/10.1002/mrm.28651. Accessed June 20, 2022. [PubMed: 33452722]
43. Fu M, Barlaz MS, Holtrop JL, et al. High-frame-rate full-vocal-tract 3D dynamic speech imaging. Magn. Reson. Med 2017;77(4):1619–1629. Available at: https://onlinelibrary.wiley.com/doi/full/10.1002/mrm.26248. Accessed June 20, 2022. [PubMed: 27099178]
44. Li G, Wei J, Kadbi M, et al. Novel Super-Resolution Approach to Time-Resolved Volumetric 4-Dimensional Magnetic Resonance Imaging With High Spatiotemporal Resolution for Multi-Breathing Cycle Motion Assessment. Int. J. Radiat. Oncol. Biol. Phys 2017;98(2):454–462. Available at: http://www.redjournal.org/article/S0360301617303942/fulltext. Accessed June 20, 2022. [PubMed: 28463165]
45. Feng L, Wen Q, Huang C, et al. GRASP-Pro: imProving GRASP DCE-MRI through self-calibrating subspace-modeling and contrast phase automation. Magn. Reson. Med 2020;83(1):94–108. [PubMed: 31400028]
46. Seiberlich N, Breuer F, Blaimer M, et al. Self-calibrating GRAPPA operator gridding for radial and spiral trajectories. Magn. Reson. Med 2008;59(4):930–935. Available at: https://onlinelibrary.wiley.com/doi/full/10.1002/mrm.21565. Accessed February 22, 2022. [PubMed: 18383296]
47. Benkert T, Tian Y, Huang C, et al. Optimization and validation of accelerated golden-angle radial sparse MRI reconstruction with self-calibrating GRAPPA operator gridding. Magn. Reson. Med 2018;80(1):286–293. [PubMed: 29193380]
48. Zhao B, Haldar JP, Christodoulou AG, et al. Image reconstruction from highly undersampled (k, t)-space data with joint partial separability and sparsity constraints. IEEE Trans. Med. Imaging 2012;31(9):1809–1820. Available at: https://pubmed.ncbi.nlm.nih.gov/22695345/. Accessed June 22, 2022. [PubMed: 22695345]
49. Lingala SG, Hu Y, Dibella E, et al. Accelerated dynamic MRI exploiting sparsity and low-rank structure: k-t SLR. IEEE Trans. Med. Imaging 2011;30(5):1042–1054. Available at: https://pubmed.ncbi.nlm.nih.gov/21292593/. Accessed June 20, 2022. [PubMed: 21292593]

50. Ong F, Zhu X, Cheng JY, et al. Extreme MRI: Large-scale volumetric dynamic imaging from continuous non-gated acquisitions. Magn. Reson. Med 2020;84(4):1763–1780. [PubMed: 32270547]
51. Christodoulou AG, Shaw JL, Nguyen C, et al. Magnetic resonance multitasking for motion-resolved quantitative cardiovascular imaging. Nat. Biomed. Eng 2018;2(4):215–226. [PubMed: 30237910]
52. Wang N, Gaddam S, Wang L, et al. Six-dimensional quantitative DCE MR Multitasking of the entire abdomen: Method and application to pancreatic ductal adenocarcinoma. Magn. Reson. Med 2020;84(2):928–948. Available at: https://pubmed.ncbi.nlm.nih.gov/31961967/. Accessed June 20, 2022. [PubMed: 31961967]
53. Lo WC, Chen Y, Jiang Y, et al. Realistic 4D MRI abdominal phantom for the evaluation and comparison of acquisition and reconstruction techniques. Magn. Reson. Med 2019;81(3):1863–1875. Available at: https://onlinelibrary.wiley.com/doi/full/10.1002/mrm.27545. Accessed June 20, 2022. [PubMed: 30394573]
54. Otazo R, Candès E, Sodickson DK. Low-rank plus sparse matrix decomposition for accelerated dynamic MRI with separation of background and dynamic components. Magn. Reson. Med 2015;73(3):1125–1136. Available at: https://pubmed.ncbi.nlm.nih.gov/24760724/. Accessed August 5, 2022. [PubMed: 24760724]
55. Feng L, Liu F, Soultanidis G, et al. Magnetization-prepared GRASP MRI for rapid 3D T1 mapping and fat/water-separated T1 mapping. Magn. Reson. Med 2021;86(1):97–114. Available at: https://onlinelibrary.wiley.com/doi/full/10.1002/mrm.28679. Accessed June 11, 2021. [PubMed: 33580909]
56. Feng L, Chandarana H, Sodickson DK, et al. Unstreaking: Radial MRI with Automatic Streaking Artifact Reduction. In Proceedings of the 25th Annual Meeting of ISMRM, Honolulu, HI, USA, 2017. p. 4001.
57. Xu B, Spincemaille P, Chen G, et al. Fast 3D contrast enhanced MRI of the liver using temporal resolution acceleration with constrained evolution reconstruction. Magn. Reson. Med 2013;69(2):370–381. Available at: https://onlinelibrary.wiley.com/doi/full/10.1002/mrm.24253. Accessed September 29, 2022. [PubMed: 22442108]
58. Chen Y, Lee GR, Wright KL, et al. Free-breathing liver perfusion imaging using 3-dimensional through-time spiral generalized autocalibrating partially parallel acquisition acceleration. Invest. Radiol 2015;50(6):367–375. Available at: https://journals.lww.com/investigativeradiology/Fulltext/2015/06000/Free_Breathing_Liver_Perfusion_Imaging_Using.1.aspx. Accessed September 29, 2022. [PubMed: 25946703]
59. Rosenzweig S, Uecker M. Ungated time-resolved cardiac MRI with temporal subspace constraint using SSA-FARY SE. In: ISMRM 2021 Annual Meeting Proceedings, Virtual. 227.
60. Wybranski C, Siedek F, Damm R, et al. Respiratory motion artefacts in Gd-EOB-DTPA (Primovist/Eovist) and Gd-DOTA (Dotarem)-enhanced dynamic phase liver MRI after intensified and standard pre-scan patient preparation: A bi-institutional analysis. PLoS One 2020;15(3). Available at: /pmc/articles/PMC7083299/. Accessed June 22, 2022.

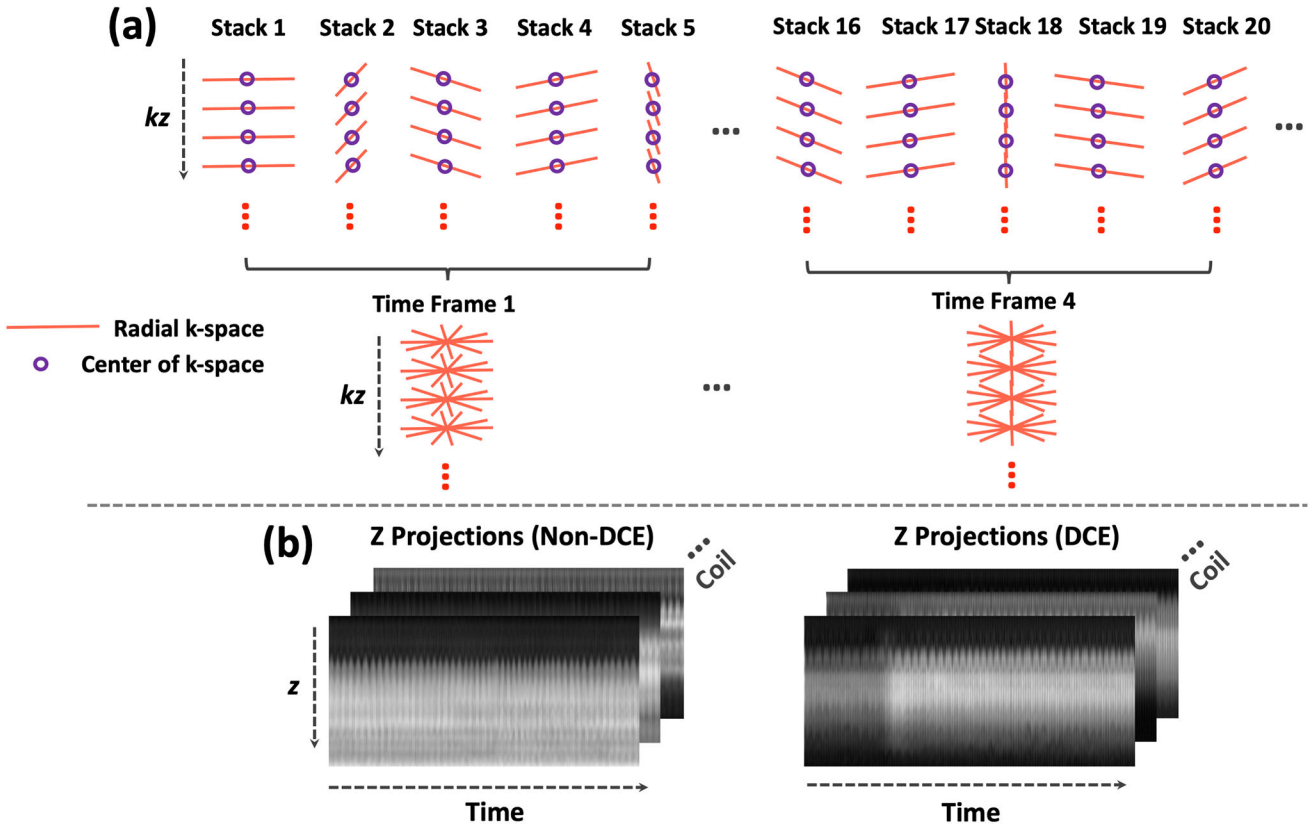

Figure 1.

(a) In stack-of-stars radial imaging, the centers of k-space in each radial stack (purple circles) can form a z-directional projection after performing 1D FFT. These projections, when plotted along time, reflect temporal variation for estimating different information, such as respiratory motion and temporal basis functions. In particular, a temporal basis can be used to construct a subspace for low-rank subspace constraint in image reconstruction. When golden-angle radial sampling is implemented, several consecutive spokes can be combined to form a dynamic frame, and a 4D dynamic image series can be reconstructed with high temporal resolution. (b) Two examples of z-directional projection profiles, one without contrast injection (left) and one with contrast injection (right).

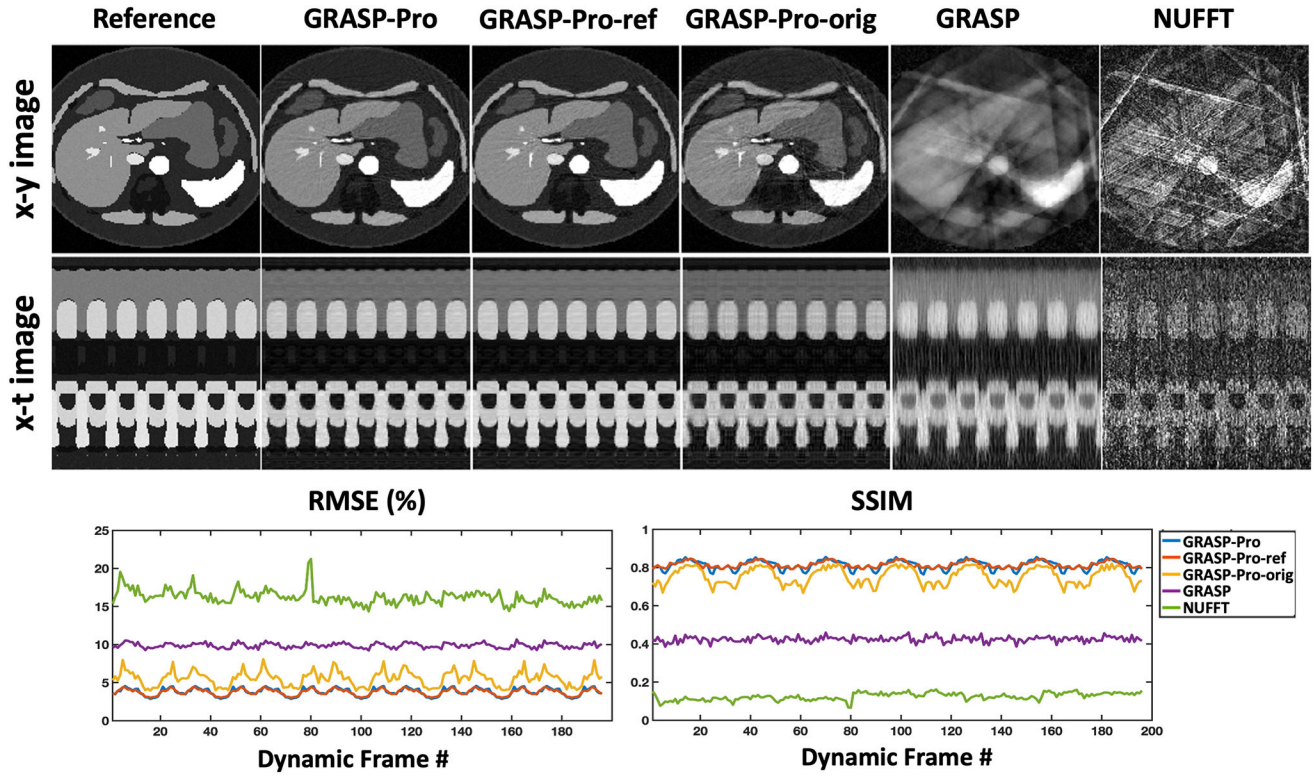

Figure 2.

(a) Comparison of NUFFT, GRASP and GRASP-Pro reconstruction with different basis estimation schemes (GRASP-Pro-ref: from fully sampled images; GRASP-Pro: from stack-of-stars k-space centers; GRASP-Pro-orig: from an intermediate reconstruction step). Image reconstruction was performed with 5 spokes grouped in each dynamic frame in each slice using the stack-of-stars golden-angle radial trajectory. NUFFT reconstruction yielded substantial undersampling artifacts. GRASP reconstruction failed to remove artifacts. GRASP-Pro-ref and GRASP-Pro reconstruction were able to recover images with comparable image quality with respect to the reference. GRASP-Pro-orig achieved compromised reconstruction performance. The RMSE and SSIM for each dynamic frame were plotted for each reconstruction method.

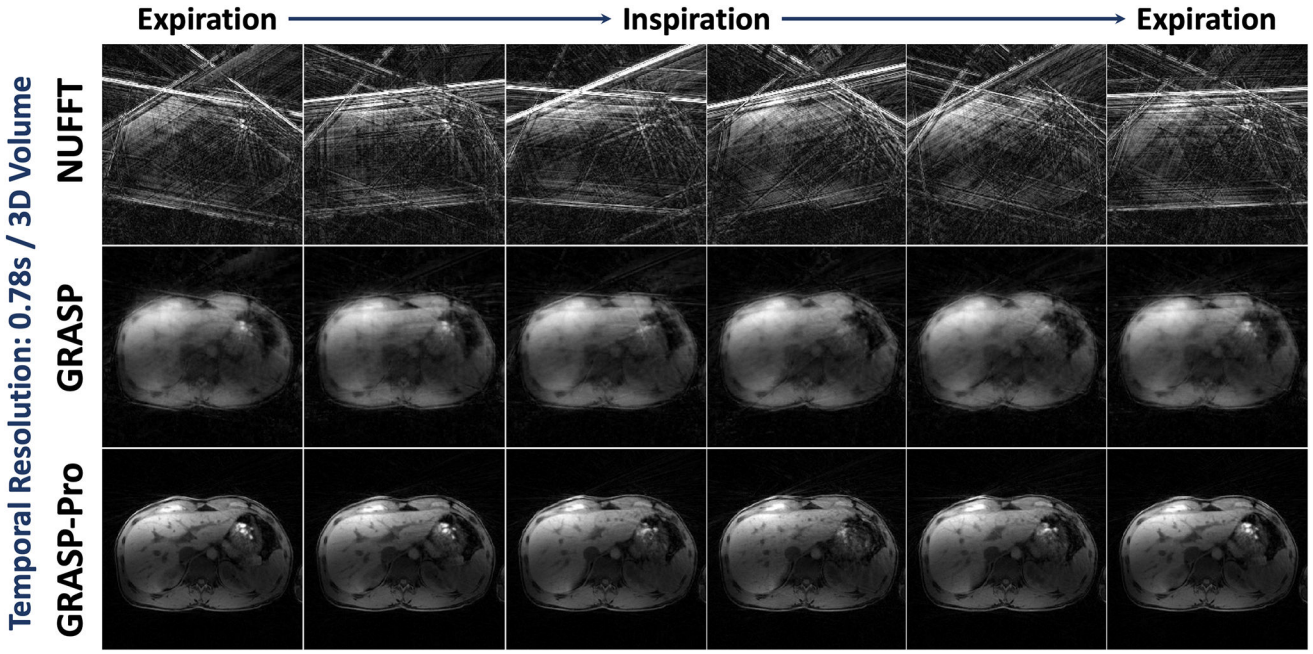

Figure 3.

Comparison of NUFFT, GRASP and GRASP-Pro reconstruction for 4D dynamic MRI (one representative slice) for non-DCE dataset 1. For each slice of the stack-of-stars dataset, image reconstruction was performed with only 5 spokes in each temporal frame, leading to a temporal resolution of 0.78 seconds/3D volume. NUFFT reconstruction produced substantial streaking artifacts. Although GRASP could remove some artifacts, the reconstruction quality remains low. In comparison, GRASP-Pro was able to reconstruct clean and sharp images with good delineation of image structures in different temporal frames.

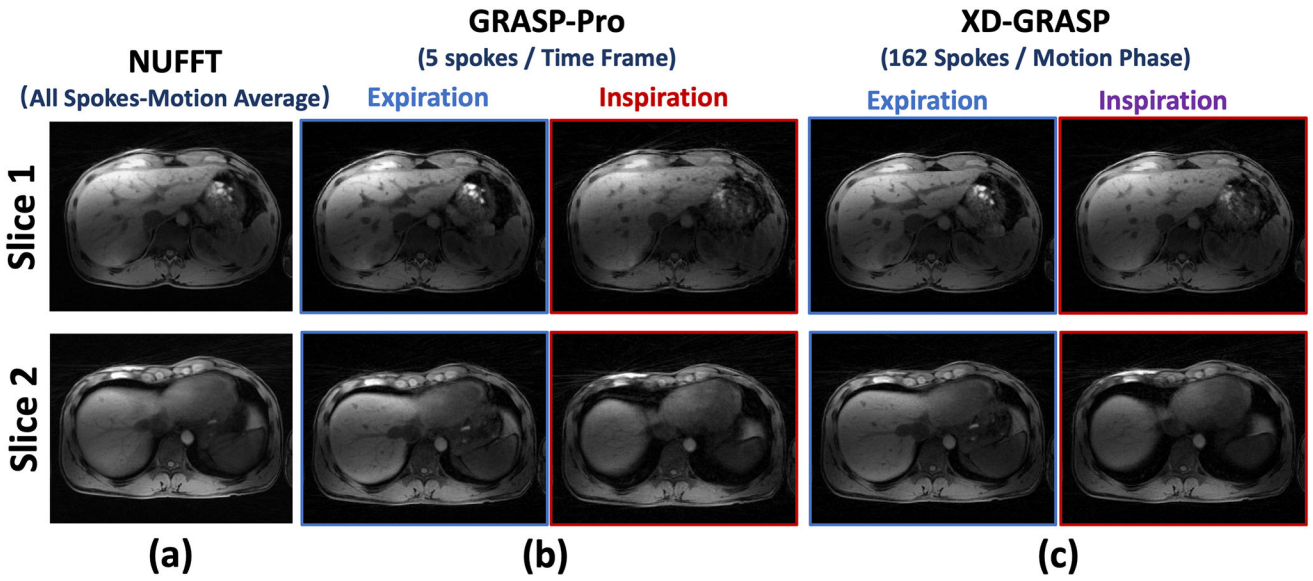

Figure 4.

Comparison of motion-averaged NUFFT reconstruction using all the acquired spokes, 4D dynamic images reconstructed using GRASP-Pro (5 spokes each temporal frame) and 4D respiratory-resolved images reconstructed using XD-GRASP (162 spokes each respiratory phase) in non-DCE dataset 1. Both expiratory and inspiratory images are displayed for GRASP-Pro and XD-GRASP reconstruction. Compared to motion-averaged reconstruction, both GRASP-Pro and XD-GRASP reconstruction yielded improved image sharpness as indicated by the better delineated vessel-tissue boundaries.

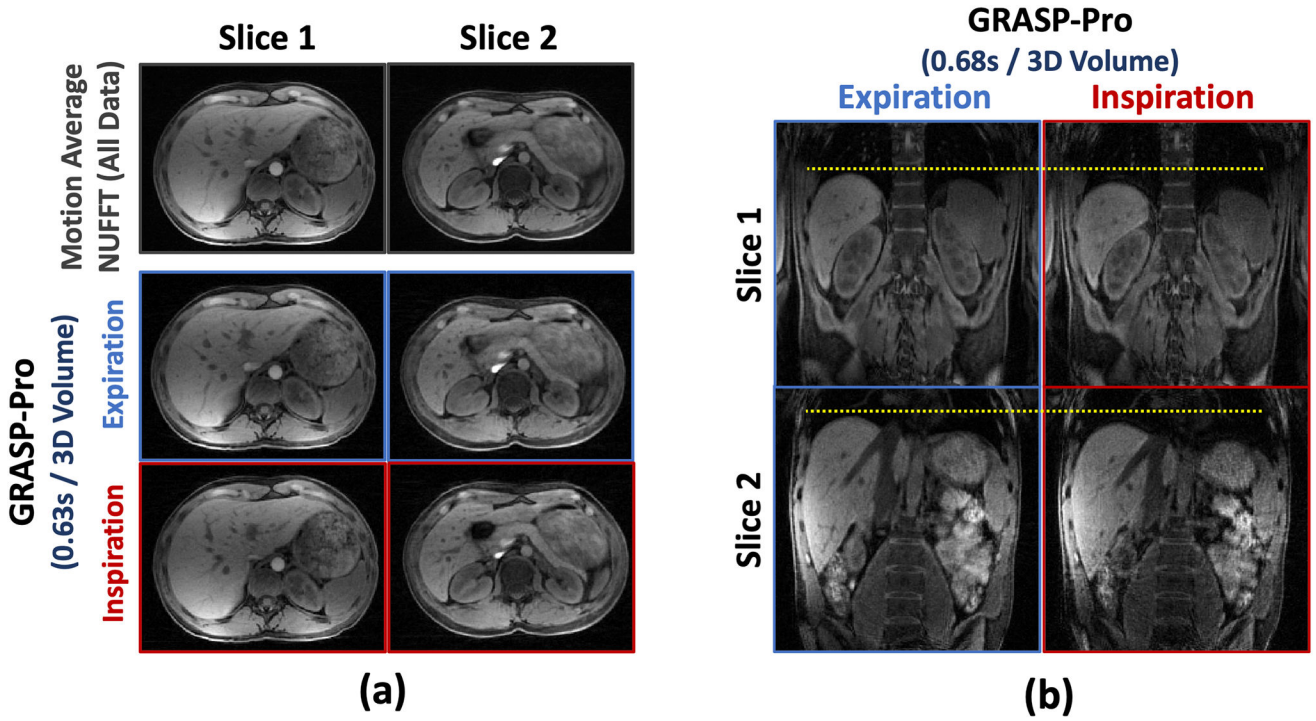

Figure 5.

4D dynamic images (both expiratory and inspiratory phases) reconstructed using GRASP-Pro for non-DCE dataset 2 and non-DCE dataset 3 with 5 spokes grouped in each temporal frame in each slice. The temporal resolution is 0.63 seconds/3D volume (axial imaging) and 0.68 seconds/3D volume (coronal imaging).

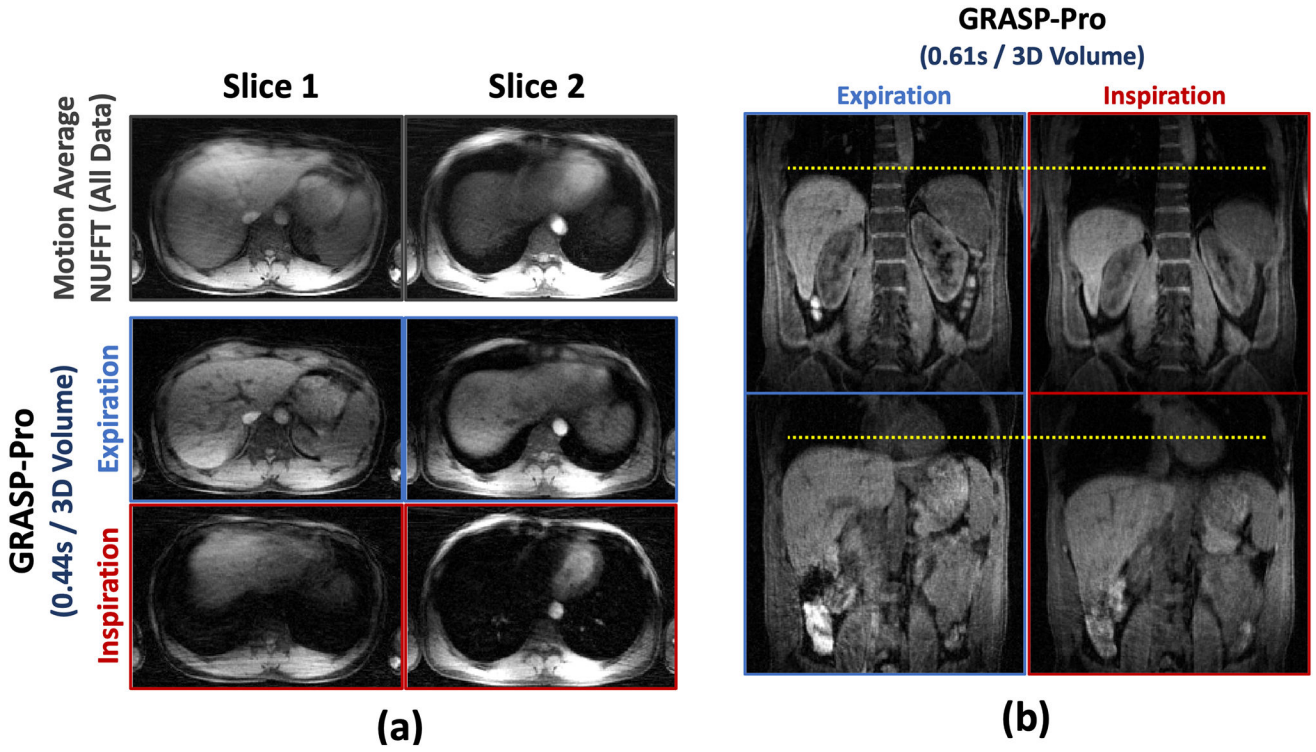

Figure 6.

GRASP-Pro reconstruction in non-DCE dataset 4 and non-DCE dataset 5 with consistent deep breathing. The temporal resolution is 0.44 seconds/3D volume for the axial images and is 0.61 seconds/3D volume for the coronal images. Although the overall image quality is reduced compared to normal breathing (non-DCE dataset 1–3), GRASP-Pro was still able to reconstruct good images, especially compared to the motion-averaged images with strong respiratory blurring.

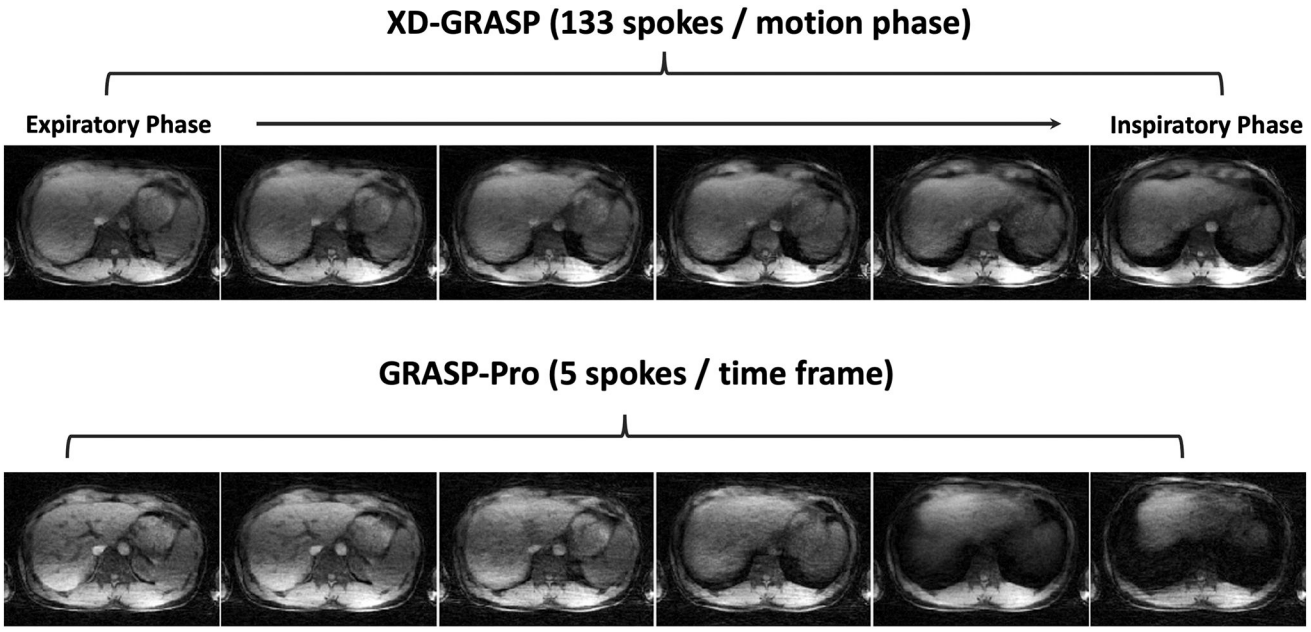

Figure 7.

Comparison of XD-GRASP with GRASP-Pro in non-DCE dataset 4 with deep breathing. XD-GRASP with the typical 6 motion-phase reconstruction is insufficient to fully resolve respiratory motion, while GRASP-Pro with a sub-second temporal resolution was able to recover more details in the liver.

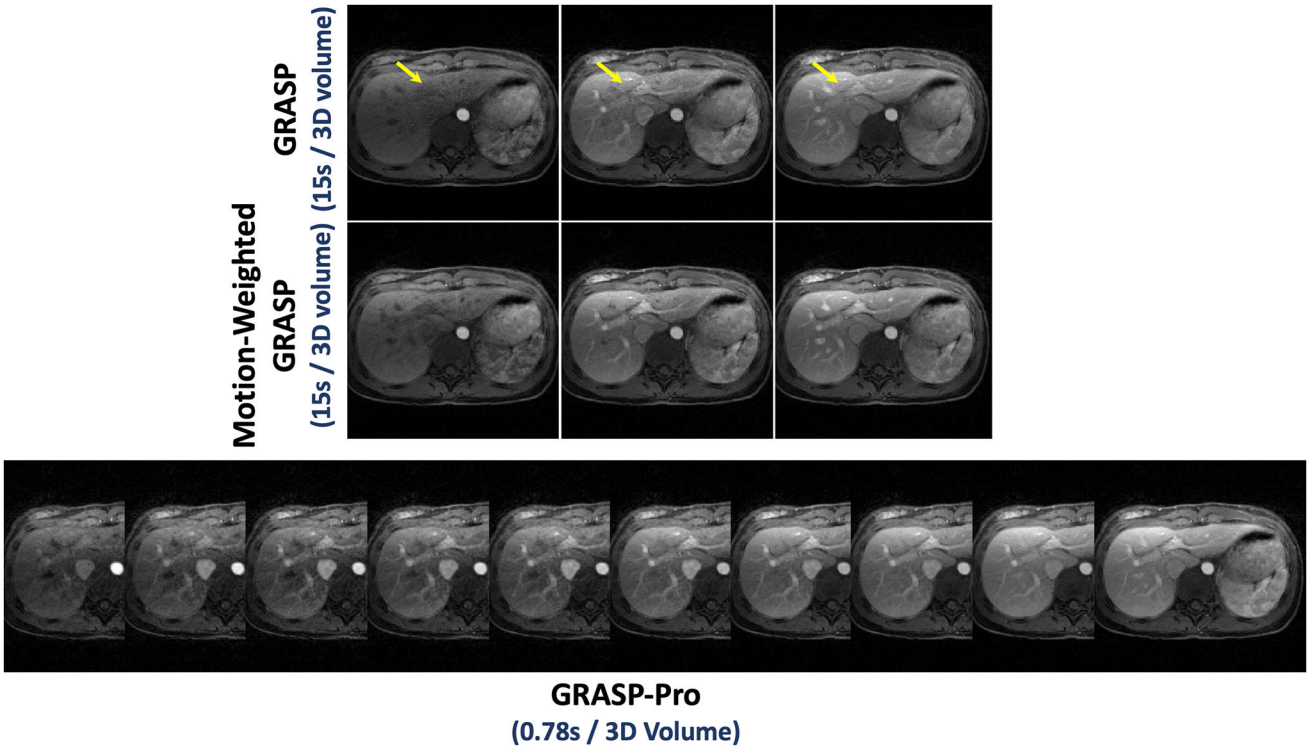

Figure 8.

Comparison of low-temporal-resolution GRASP reconstruction (15 seconds/3D volume) and motion-weighted GRASP reconstruction (15 seconds/3D volume) with high-temporal-resolution GRASP-Pro reconstruction (0.78 seconds/3D volume) in DCE dataset 1. GRASP-Pro reconstruction did not implement any motion compensation algorithm and only expiratory phases are displayed. Despite substantially higher temporal resolution (0.78 seconds/3D volume verse 15 seconds/3D volume), GRASP-Pro reconstruction still led to good reconstruction quality compared to motion-weighted GRASP reconstruction, and standard GRASP reconstruction suffers from residual motion blurring as indicated by the blurred hepatic vessels (yellow arrows).

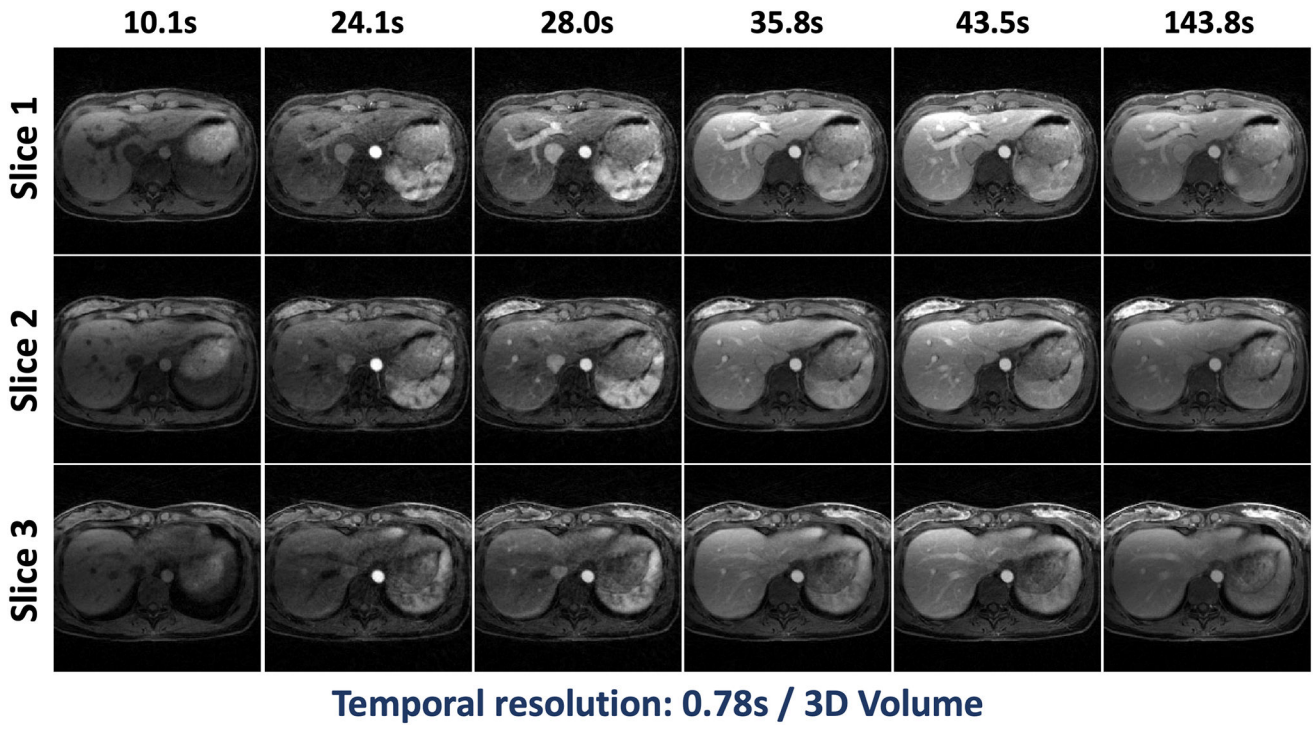

Figure 9.
Three slices of different contrast phases in DCE dataset 1 reconstructed using GRASP-Pro with a temporal resolution of 0.78 seconds/3D volume.

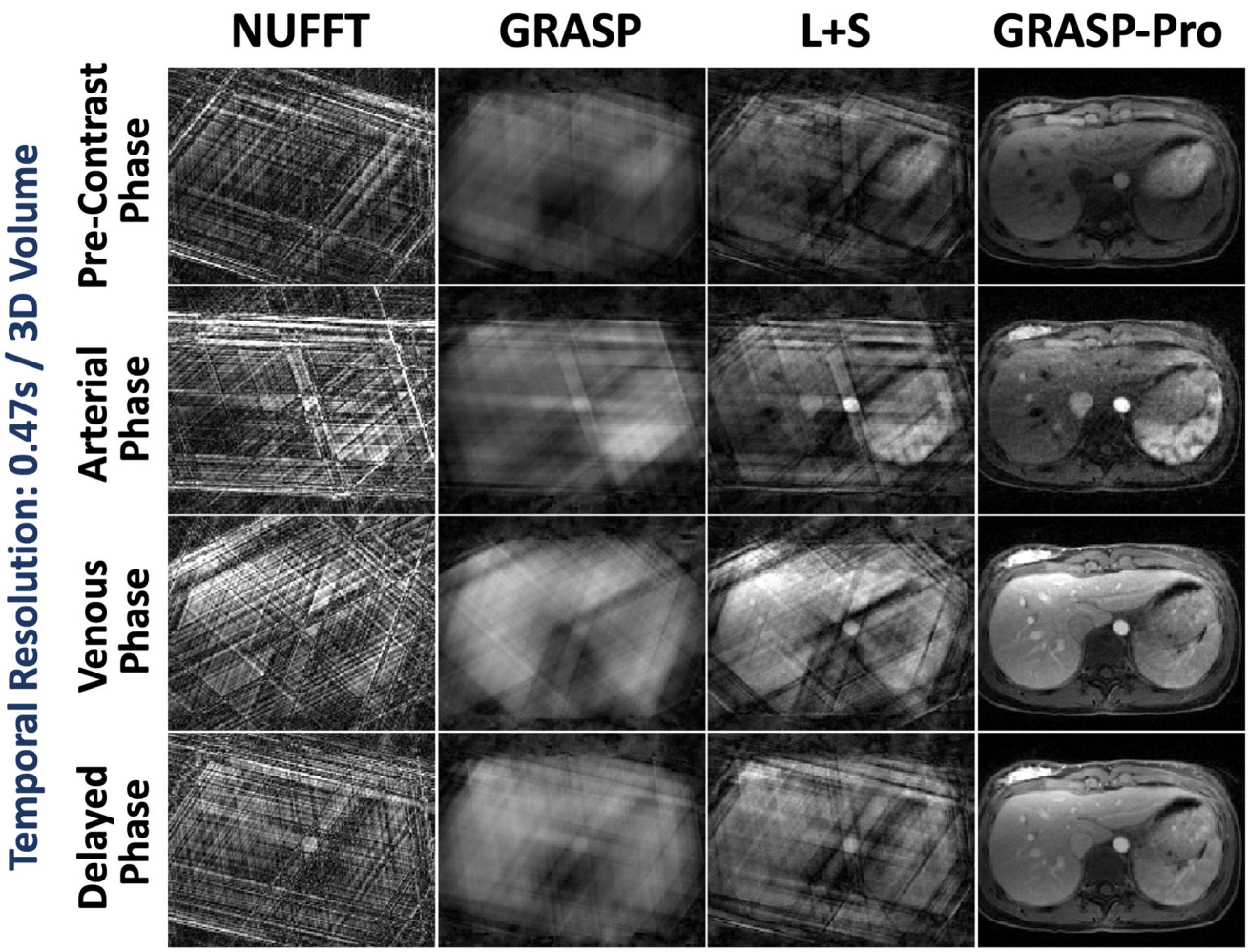

Figure 10.

Comparison of NUFFT, GRASP, L+S and GRASP-Pro reconstruction for 4D dynamic MRI (one representative slice) for DCE dataset 1. For each slice of the stack-of-stars dataset, image reconstruction was performed with only 3 spokes in each temporal frame, leading to a temporal resolution of 0.47 seconds/3D volume. NUFFT reconstruction produced strong streaking artifacts. Although GRASP and L+S could remove some artifacts, the reconstruction quality remains low. In comparison, GRASP-Pro was able to reconstruct clean and sharp images with good delineation of image structures in different contrast-enhanced phases.

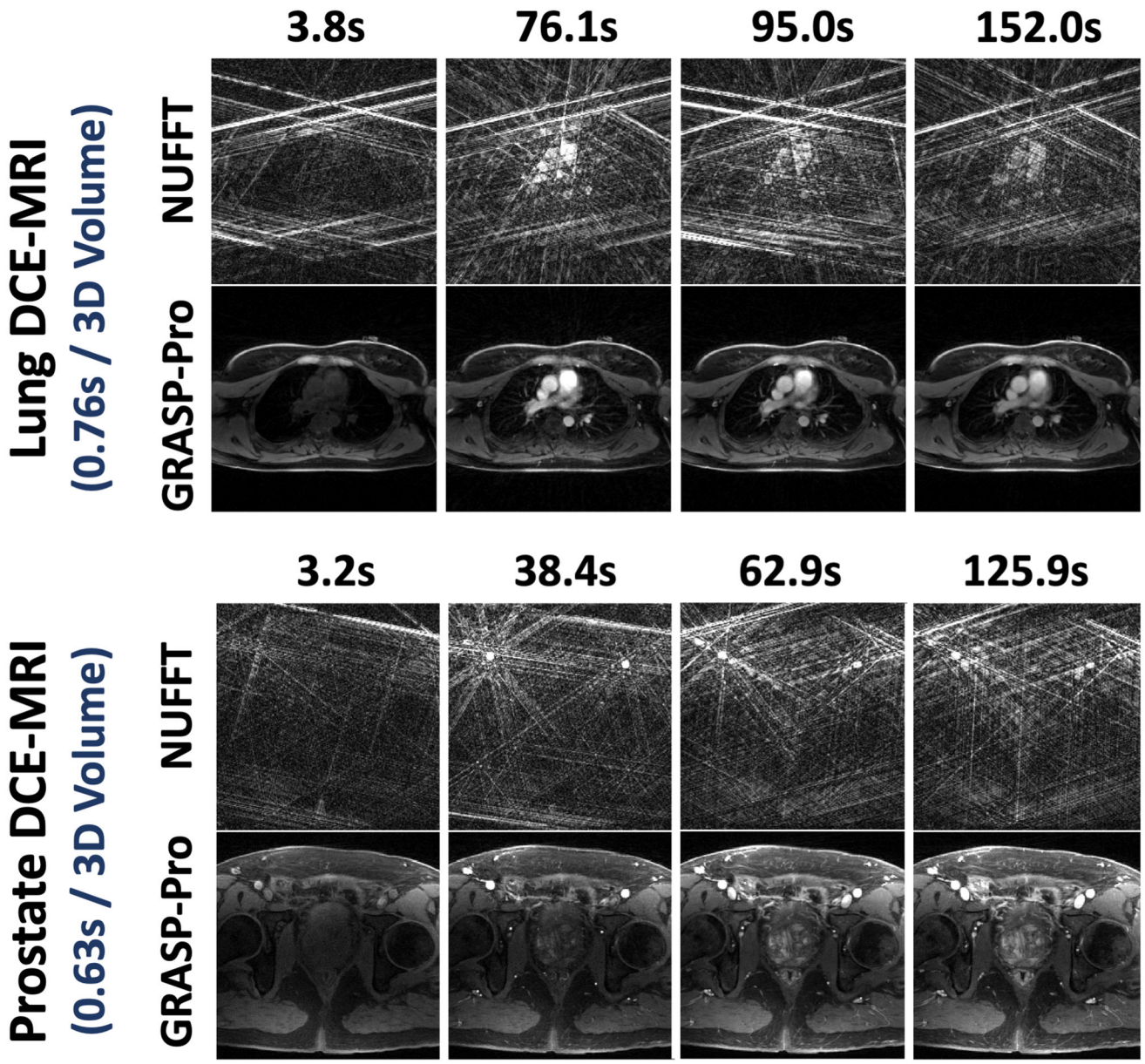

Figure 11.

GRASP-Pro reconstruction in DCE dataset 2 (upper panel, lung imaging) and DCE dataset 3 (lower panel, prostate imaging) showing the recovery of image quality from NUFFT reconstruction with 5 spokes per temporal frame in each slice. The temporal resolution is 0.76 seconds/3D volume for the lung images and is 0.63 seconds/3D volume for the prostate images.

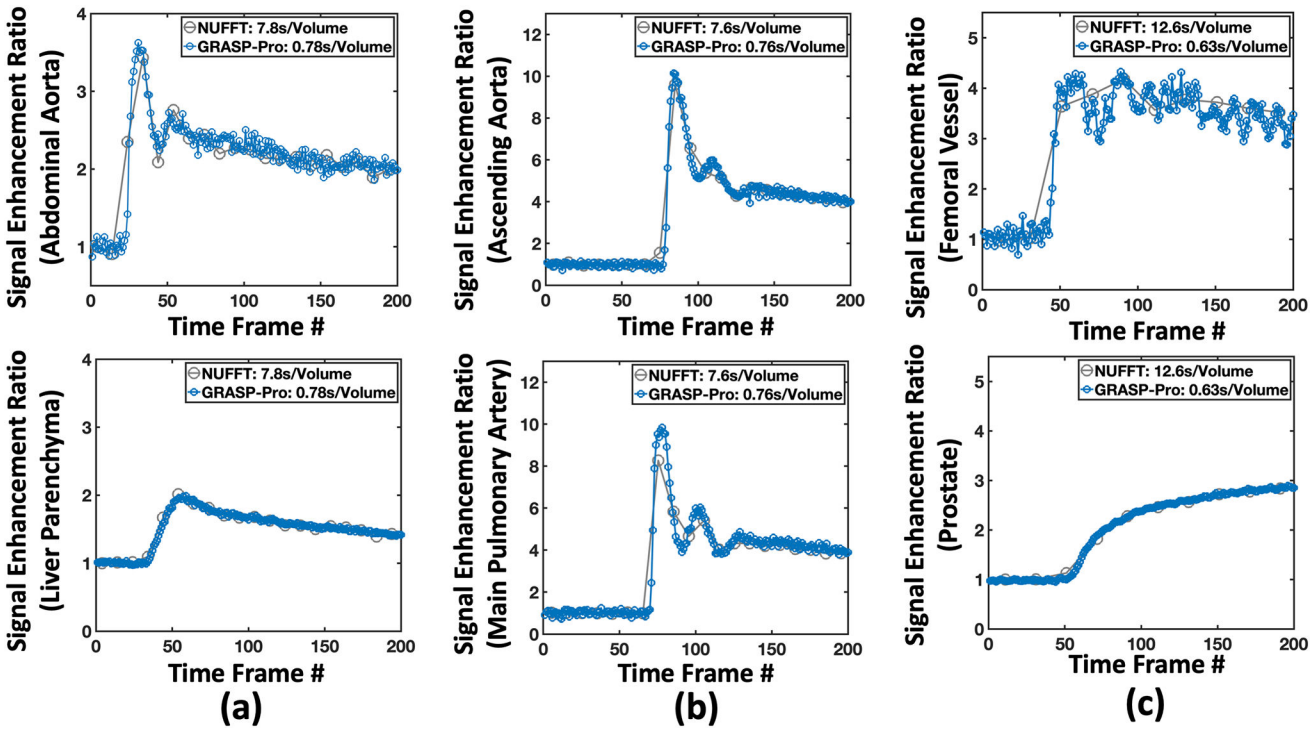

Figure 12.

Contrast enhancement curves from the 4D DCE-MRI of the liver, the lung and the prostate reconstructed using GRASP-Pro DCE datasets 1–3. For comparison and validation, corresponding contrast enhancement curves from the 4D DCE-MRI reconstructed using NUFFT with a lower temporal resolution (as indicated in the figure legend) are also displayed. Although the NUFFT images have streaking artifacts, temporal fidelity is expected preserved in ROI-averaged contrast enhancement curves.

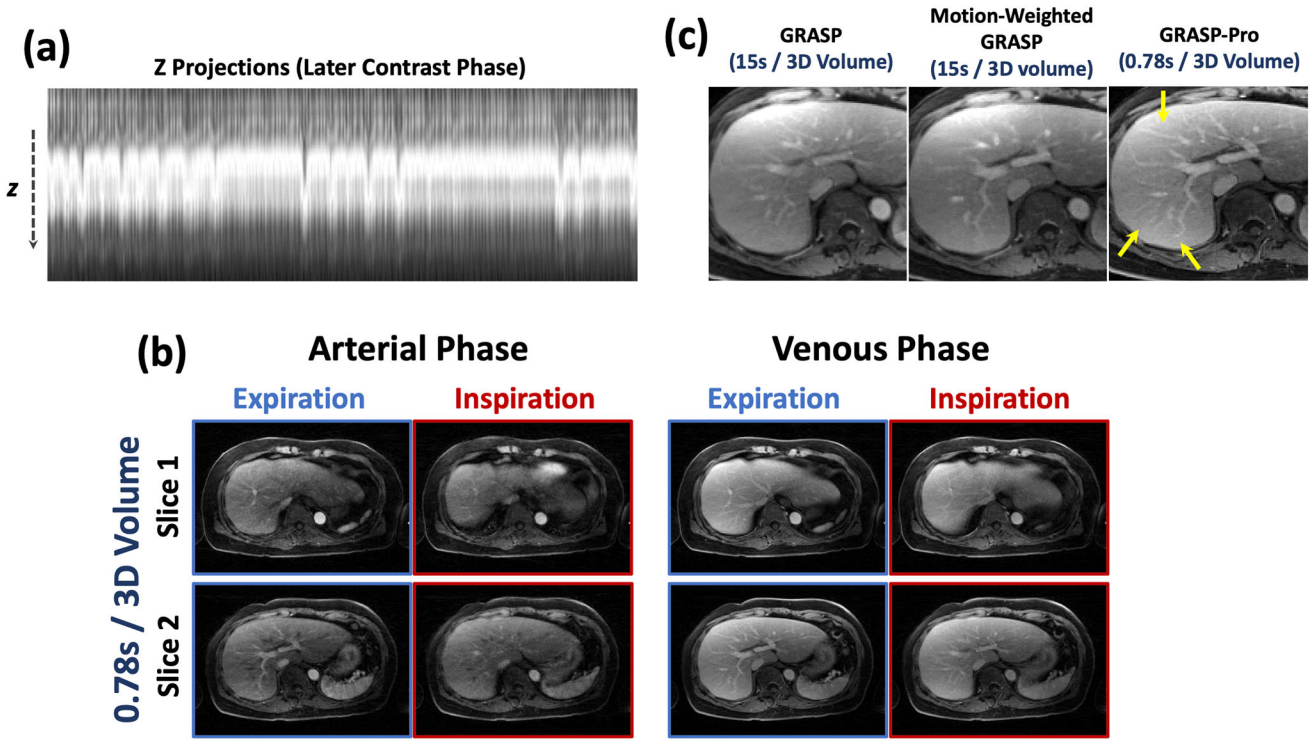

Figure 13.

GRASP-Pro reconstruction in DCE dataset 4. (a) the z projection profiles show that the subject had irregular breathing during data acquisition. (b) GRASP-Pro was able to reconstructed good images in different contrast phases with a temporal resolution of 0.78 seconds/3D volume. (c) Comparison of low-temporal-resolution GRASP reconstruction (15 seconds/3D volume) and motion-weighted GRASP reconstruction (15 seconds/3D volume) with high-temporal-resolution GRASP-Pro reconstruction (0.78 seconds/3D volume) in a venous contrast phase. GRASP-Pro was able to recover small details (small vessels) that are blurred in GRASP and motion-weighted GRASP (likely due to motion and irregular breathing from low-temporal-resolution reconstruction).

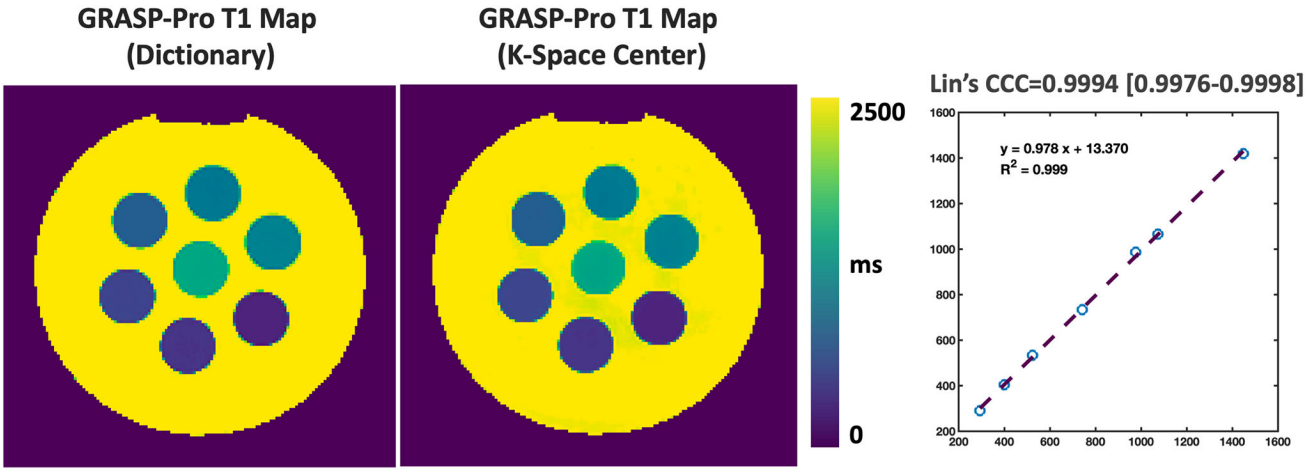

Figure 14.

Comparison of T1 maps generated from images reconstructed with GRASP-Pro using a temporal basis estimated from a dictionary generated using the Bloch equations and a temporal basis estimated from the centers of k-space. There is no visual difference in the T1 maps, which is confirmed by the quantitative analysis of mean T1 values in different phantom vials.

Table 1:

Imaging parameters for different non-DCE-MRI and DCE-MRI datasets.

	Matrix Size	FOV (mm^2)	Slice Thickness (mm)	TR/TE (ms)	FA (degree)	Slice PF	Total Spokes Per Slice	Number of Slices	Scan Time (s)
Non-DCE Data 1	256×256	350×350	5	3.62/1.57	12	80%	650	38	102
Non-DCE Data 2	192×192	300×300	5	3.52/1.49	12	80%	800	28	100
Non-DCE Data 3	256×256	340×340	5	4.18/1.49	12	80%	1200	26	163
Non-DCE Data 4	192×192	360×360	5	3.43/1.43	12	80%	800	20	70
Non-DCE Data 5	192×192	360×360	5	3.43/1.43	12	80%	1304	28	159
DCE Data 1	256×256	350×350	5	3.6/1.6	12	80%	1222	38	190
DCE Data 2	256×256	350×350	5	3.5/1.55	12	80%	1200	38	182
DCE Data 3	224×224	240×240	5	4.12/1.96	12	80%	1755	24	221
DCE Data 4	256×256	350×350	5	3.6/1.6	12	80%	1222	38	190

FOV: field of view; TR: repetition time; TE: echo time; FA: flip angle.